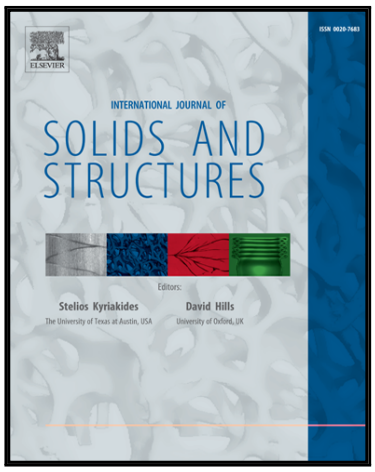

Swelling, Inflation, and a Swelling-Burst Instability in Hyperelastic Spherical Shells

Vahid Zamani, Thomas J. Pence

PII: S0020-7683(17)30327-X
DOI: 10.1016/j.ijsolstr.2017.07.010
Reference: SAS 9656

To appear in: *International Journal of Solids and Structures*

Received date: 3 May 2017
Revised date: 29 June 2017
Accepted date: 5 July 2017

Please cite this article as: Vahid Zamani, Thomas J. Pence, Swelling, Inflation, and a Swelling-Burst Instability in Hyperelastic Spherical Shells, *International Journal of Solids and Structures* (2017), doi: 10.1016/j.ijsolstr.2017.07.010

Swelling, Inflation, and a Swelling-Burst Instability in Hyperelastic Spherical Shells

Vahid Zamani[a,*], Thomas J. Pence[a]

[a]*Department of Mechanical Engineering*
Michigan State University
East Lansing, Michigan, USA

Abstract

The incompressible hyperelastic Mooney-Rivlin constitutive model allows for pressure-inflation response of spherical shells that could either be globally stable (a monotonic pressure-radius graph) or could instead involve instability jumps of various kinds as pressurization proceeds. The latter occurs when the pressure-radius graph is not monotonic, allowing for a snap-through bifurcation that gives a sudden burst of inflation. For a given structure (shell thickness) composed of a specific material (a parameter choice in the M-R constitutive model), the form of the pressure-radius graph becomes fixed, enabling the determination of whether and when such a burst will be triggered. Internal swelling of the material that makes up the shell wall will generally change the response. Not only does it alter the quantitative pressure-inflation relation but it can also change the qualitative stability response, allowing burst phenomena for certain ranges of swelling and preventing burst phenomena for other ranges of swelling. This paper provides a systematic framework for predicting how such swelling ranges depend on structural geometry and material parameters.

Keywords: hyperelasticity, swelling, shells, burst

1. Introduction

Soft matter swells, causing quantitative changes in the material's mechanical properties. These can lead to qualitative changes in the stability of the overall structure, possibly triggering various bifurcation phenomena associated with localization, buckling and other forms

*Corresponding author
Email address: zamaniva@msu.edu (Vahid Zamani)

of nonuniqueness. Here we examine how swelling affects the inflation response of hyperelastic spheres. The inflation response of a hyperelastic sphere in the absence of swelling is a classical problem in finite deformation continuum mechanics. As is well known, the resulting presssure-expansion response is not always given by a monotonically increasing graph. When this happens, various inflation jump events can be triggered. The intent of this work is to examine how swelling affects this response.

For our purposes, swelling is regarded as a general process that encompasses free-volume change at the microscopic level. This would typically be due to mass addition resulting from some diffusive or transport mechanism, but other fine scale processes of a mechanical or chemical nature can also be regarded as contributing to volume change. Polymers, elastomers and hydrogels naturally swell when exposed to liquid or when subject to high humidity Treloar (1975); Stuart et al. (2010); Drozdov (2013). Biological tissues and cells exhibit volume and shape change under similar processes of hydration and mass exchange Van der Sman (2015), but also more generally as a result of biological growth Goriely et al. (2010); Sadik et al. (2016). In many cases osmotic pressure is the causal agent that drives water and other mass transport across bio-membranes such as those surrounding red blood cells and intercellular vesicles Graf et al. (1995); Vinod Kumar & Demeke (2011); Li et al. (2013). The mechanical consequences of these processes in terms of deformability, instability, limiting stretch and possible rupture are significant Evans et al. (2003); Gibbons & Klug (2008); Nagel et al. (2009).

Here we focus attention on a class of swellable hyperelastic materials in order to examine how the constitutive theory affects the spherically symmetric expansion of a pressurized hollow sphere. The sphere may be thick or thin. The thin wall limit corresponds to a hyperelastic swellable membrane. In the absence of swelling the class of materials corresponds to a classical Mooney-Rivlin material. The inflation response for a hollow sphere composed of the classical Mooney-Rivlin material has been extensively studied. We especially focus on a detailed characterization by Carroll Carroll (1987) that provides conditions that determine when the inflation response is monotone versus when it is not. We use this characterization to describe the non-swelling response of the sphere problem under consideration here. We then generalize the analysis so as to determine how swelling affects the outcome. In particular, we exhibit swelling induced transitions between monotone and non-monotone inflation curves. We provide a systematic framework for understanding and predicting these transitions, and we discuss the ramifications of these transitions in terms of a snap-through

type bifurcation (a swelling induced burst).

2. Preliminaries

The continuum mechanical treatment of finite deformation describes how locations $\mathbf{X}$ in a reference configuration Ω_X are mapped into deformed locations $\mathbf{x}$ in the current configuration Ω_x. The gradient of the map $\mathbf{x} = \chi(\mathbf{X})$ is the tensor

$$\mathbf{F} = \partial\mathbf{x}/\partial\mathbf{X}. \tag{1}$$

In this work we focus attention on changes in the material's natural free volume and this allows the material to expand and contract. This volume change is typically due to a mass addition such as fluid absorption, however other mechanisms of volume change can be treated by the present framework. Whatever the cause, this volume change can vary from point to point and is described with the aid of a *swelling field* $v = v(\mathbf{X})$.

In the absence of volume change $v = 1$, whereas volume increase (or decrease) gives v greater (or less) than one. In the present treatment this generates a volume constraint on the deformation in the form

$$\det\mathbf{F} = v. \tag{2}$$

A theory that uses (2) provides a generalization of the conventional theory for incompressible materials. For example, such a treatment is employed in Tsai et al. (2004) to analyze how nonhomogeneous swelling fields induce flexure deformations in a rectangular block.

The energetic framework is based on a hyperelastic elastic energy density Was a function of both $\mathbf{F}$ and v. The energy density is frame invariant and this requires W to depend on $\mathbf{F}$ only through the right Cauchy-Green deformation tensor $\mathbf{C} = \mathbf{F}^T\mathbf{F}$. In the absence of body forces the equilibrium equation is $div\mathbf{T} = 0$ where $\mathbf{T}$ is the Cauchy stress tensor:

$$\mathbf{T} = \frac{2}{v}\mathbf{F}\frac{\partial W}{\partial \mathbf{C}}\mathbf{F}^T - p\mathbf{I}. \tag{3}$$

Here p is the hydrostatic pressure associated with the volume constraint (2). Attention is restricted to isotropic materials so that the dependence of W on $\mathbf{C}$ is in terms of its invariants $I_1 = \operatorname{tr}\mathbf{C} = \lambda_1^2 + \lambda_2^2 + \lambda_3^2$ and $I_2 = \frac{1}{2}\big((\operatorname{tr}\mathbf{C})^2 - \operatorname{tr}\mathbf{C}^2\big) = \lambda_1^2\lambda_2^2 + \lambda_2^2\lambda_3^2 + \lambda_3^2\lambda_1^2$. Here $\lambda_i > 0$ $(i = 1, 2, 3)$ are the principal stretches as measured from the unswollen reference

configuration (λ_i^2 are the eigenvalues of $\mathbf{C}$). The third invariant $I_3 = \det \mathbf{C}$ is equal to v^2 by virtue of (2). We shall use notation $W = W(I_1, I_2, v)$ and $W = \bar{W}(\lambda_1, \lambda_2, \lambda_3, v)$ in what follows.

The Cauchy stress tensor $\mathbf{T}$ is symmetric and its eigenvalues are the principle stresses, denoted by T_1, T_2 and T_3. In the absence of swelling a standard requirement on any isotropic hyperelastic constitutive model is the well known Baker-Ericksen inequality

$$(T_i - T_j)(\lambda_i - \lambda_j) > 0, \qquad (i \neq j, \lambda_i \neq \lambda_j, \text{no sum}). \tag{4}$$

This is a requirement that the maximum (minimum) principle stress direction correlates with the maximum (minimum) stretch direction. For a swellable isotropic material the same logic continues to apply and so we presume that (4) holds for the materials under consideration here.

The particular constitutive model that will be used for specific examples in this paper is motivated by the well known Mooney-Rivlin model

$$W_{\text{MR}}(I_1, I_2) = d_1(I_1 - 3) + d_2(I_2 - 3), \tag{5}$$

in the classical incompressible theory where the positive constants d_1 and d_2 are empirically determined material parameters. The generalization of the Mooney-Rivlin model for swelling is to keep the basic form (5) while now letting d_1 and d_2 depend upon v. For this purpose we shall in what follows consider examples using

$$W(I_1, I_2, v) = d_1\left(\frac{I_1}{v^{2/3}} - 3\right) + d_2\left(\frac{I_2}{v^{4/3}} - 3\right), \;\; d_1 = d_1(v), \;\; d_2 = d_2(v), \tag{6}$$

with $d_1 \geq 0$, $d_2 \geq 0$ and $d_1 + d_2 > 0$. The reason for the scalings $I_1/v^{2/3}$ and $I_2/v^{4/3}$ in (6) is that $I_1/v^{2/3} = I_2/v^{4/3} = 3$ for an equiaxial free expansion $\mathbf{F} = v^{1/3}\mathbf{I}$. This enables certain algebraic simplifications.

When (6) holds the Cauchy stress tensor (3) becomes

$$\mathbf{T} = 2\left(\frac{d_1}{v^{5/3}} + I_1\frac{d_2}{v^{7/3}}\right)\mathbf{b} - 2\frac{d_2}{v^{7/3}}\mathbf{b}^2 - p\mathbf{I}, \qquad \mathbf{b} = \mathbf{F}\mathbf{F}^T. \tag{7}$$

Calculating T_i and T_j from (7) one then obtains

$$T_i = 2\left(\frac{d_1}{v^{5/3}} + (\lambda_j^2 + \lambda_k^2)\frac{d_2}{v^{7/3}}\right)\lambda_i^2 - p, \qquad (i \neq j \neq k \neq i). \tag{8}$$

Using this result it follows for the material model (6) that

$$(T_i - T_j)(\lambda_i - \lambda_j) = 2\left(\frac{d_1}{v^{5/3}} + \lambda_k^2\frac{d_2}{v^{7/3}}\right)(\lambda_i - \lambda_j)^2(\lambda_i + \lambda_j) \tag{9}$$

Thus the Baker-Ericksen type condition (4) is automatically satisfied when W is given by (6) because $d_1 \geq 0$ and $d_2 \geq 0$.

Constitutive laws similar to (6) have previously been used to study a variety of boundary value problems involving mass addition and volumetric change. This includes the studies of Pence and Tsai on swelling induced cavity formation in tubes Pence & Tsai (2005) and spheres Pence & Tsai (2006). Amar and Goriely Ben Amar & Goriely (2005) make use of a constant material parameter version of (6) in the context of more generalized processes of growth to investigate instabilities in the inflation response of spherical shells when the shell wall experiences anisotropic growth. The study Demirkoparan & Pence (2008) analyzes swelling induced twist in fiber reinforced composites for materials where the matrix constituent swells (and is described by (6)) but the fibrous constituent does not swell and so admits to an alternative constitutive law. In this paper we will ultimately make use of (6) to study the interaction of swelling and pressure on the inflation response of thick walled spheres when the material parameters d_2 and d_2 are also swelling dependent.

3. Kinematics for radial inflation of a spherical shell

Using the framework just described in Section 2 we consider a finite thickness spherical shell with inner radius $R_i > 0$ and outer radius $R_o > R_i$ prior to any loading or any swelling. Attention is restricted to radially symmetric swelling $v = v(R)$. The loading is taken to consist of applied pressures P_i and P_o on the inner and outer boundaries. These symmetric conditions motivate the consideration of the symmetric deformation for *radial inflation*

$$r = r(R), \quad \theta = \Theta, \quad \phi = \Phi \tag{10}$$

on $R_i \leq R \leq R_o$, $0 \leq \Theta < 2\pi$, $0 \leq \Phi \leq \pi$ where the radial inflation function $r(R)$ is to be determined. Thus (10) is a map from reference spherical coordinates (R, Θ, Φ) to deformed spherical coordinates (r, θ, ϕ). Let $\{\mathbf{e}_R, \mathbf{e}_\Theta, \mathbf{e}_\Phi\}$ represent the unit basis vectors in the reference configuration and let $\{\mathbf{e}_r, \mathbf{e}_\theta, \mathbf{e}_\phi\}$ represent the unit basis vectors in the deformed configuration. It follows from (10) that the deformation gradient is given by $\mathbf{F} = \lambda_r(\mathbf{e}_r \otimes \mathbf{e}_R) + \lambda_\theta \mathbf{e}_\theta \otimes \mathbf{e}_\Theta + \lambda_\phi \mathbf{e}_\phi \otimes \mathbf{e}_\Phi$ with

$$\lambda_r = r' \quad \text{and} \quad \lambda_\theta = \lambda_\phi = r/R \tag{11}$$

in which prime $'$ denotes the differentiation with respect to R ($r' = dr/dR$). The swelling constraint (2) is

$$v = \frac{r^2 r'}{R^2}, \tag{12}$$

Integrating (12) from the inner radius R_i to a generic radial value R gives

$$r^3 = r_i^3 + 3\int_{R_i}^{R} v(\zeta)\zeta^2 d\zeta \tag{13}$$

where $r_i = r(R_i)$. More generally (13) provides the map $r = r(R)$ in terms of the single parameter r_i which still needs to be determined. The Cauchy stress tensor takes the form

$$\mathbf{T} = T_{rr}(\mathbf{e}_r \otimes \mathbf{e}_r) + T_{\theta\theta}(\mathbf{e}_\theta \otimes \mathbf{e}_\theta + \mathbf{e}_\phi \otimes \mathbf{e}_\phi) \tag{14}$$

with

$$\begin{aligned} T_{rr} &= \frac{2}{v}\frac{\partial W}{\partial I_1}\lambda_r^2 + \frac{4}{v}\frac{\partial W}{\partial I_2}\lambda_r^2\lambda_\theta^2 - p, \\ T_{\theta\theta} &= \frac{2}{v}\frac{\partial W}{\partial I_1}\lambda_\theta^2 + \frac{2}{v}\frac{\partial W}{\partial I_2}(\lambda_r^2 + \lambda_\theta^2)\lambda_\theta^2 - p. \end{aligned} \tag{15}$$

The equilibrium equations $div\mathbf{T} = 0$ gives that $p = p(R)$ along with the requirement

$$\frac{dT_{rr}}{dr} + \frac{2}{r}(T_{rr} - T_{\theta\theta}) = 0. \tag{16}$$

The specified pressures P_i and P_o at the inner and outer surfaces yield the boundary conditions

$$T_{rr}\big|_{r_i} = -P_i, \quad T_{rr}\big|_{r_o} = -P_o, \tag{17}$$

where $r_o = r(R_o)$.

Using (12) and (15) the equilibrium equation (16) provides an ordinary differential equation for $p(R)$ which can be integrated. The two boundary conditions (17) determine the integration constant that emerges from this integration as well as the scalar r_i. Once r_i is so determined the whole kinematics $r = r(R)$ then follows from (13) and consequently the deformation gradient tensor $\mathbf{F}$ is fully known. This constitutes the most obvious solution procedure for determining the output response $r(R)$ as a function of the input swelling field $v(R)$ and the input pressure values P_i and P_o.

There is however a shortcut that gets to the same result by making direct use of the stored energy density in terms of the principle stretches $\bar{W}(\lambda_r, \lambda_\theta, \lambda_\phi, v)$. It is based on a straight forward adaptation of a well known procedure from hyperelasticity when no swelling is present. This earlier procedure corresponds to the special case $v \equiv 1$ in the present treatment. Because $W(I_1, I_2, v) = \bar{W}(\lambda_r, \lambda_\theta, \lambda_\phi, v)$ with $\lambda_\theta = \lambda_\phi$ one may employ the chain rule for the differentiation in (15) in the form

$$\frac{\partial W}{\partial I_1} = \frac{\partial \bar{W}}{\partial \lambda_r}\frac{\partial \lambda_r}{\partial I_1} + 2\frac{\partial \bar{W}}{\partial \lambda_\theta}\frac{\partial \lambda_\theta}{\partial I_1}, \tag{18}$$

with

$$\frac{\partial \lambda_r}{\partial I_1} = \frac{\lambda_r^2 + \lambda_\theta^2}{2\lambda_r(\lambda_r^2 - \lambda_\theta^2)}, \qquad \frac{\partial \lambda_\theta}{\partial I_1} = \frac{\lambda_\theta}{2(\lambda_\theta^2 - \lambda_r^2)}. \tag{19}$$

A similar differentiation applies with respect to I_2 and on this basis one confirms that

$$T_{rr} = \frac{\lambda_r}{v}\frac{\partial \bar{W}}{\partial \lambda_r} - p, \qquad T_{\theta\theta} = T_{\phi\phi} = \frac{\lambda_\theta}{v}\frac{\partial \bar{W}}{\partial \lambda_\theta} - p. \tag{20}$$

Introduce the variable

$$s = r/R, \tag{21}$$

which, in view of (11), is the biaxial stretch $\lambda_\theta = \lambda_\phi$. Also let $s_i = r_i/R_i$ and $s_o = r_o/R_o$ and note that (13) gives

$$s_o^3 = \left(\frac{R_i}{R_o}\right)^3 s_i^3 + \frac{3}{R_o^3}\int_{R_i}^{R_o} v(R)R^2 dR. \tag{22}$$

In this regard, the following derivation will be useful for the formulations in the next section

$$\frac{ds}{dr} = \frac{ds/dR}{dr/dR} = \frac{Rr' - r}{R^2 r'} = \frac{v - s^3}{Rv}, \tag{23}$$

where the last step from the above chain of equations is due to (12). The relation (23) together with (12) gives

$$\lambda_r = r^{'} = v/s^2, \qquad \lambda_\theta = \lambda_\phi = r/R = s, \tag{24}$$

and hence $\bar{W}(\lambda_r, \lambda_\theta, \lambda_\phi, v) = \bar{W}(v/s^2, s, s, v)$. Now define

$$w(s, v) = \bar{W}(v/s^2, s, s, v) \tag{25}$$

and calculate the derivative

$$\frac{\partial w(s,v)}{\partial s} = \frac{\partial \bar{W}}{\partial \lambda_r}\frac{\partial \lambda_r}{\partial s} + 2\frac{\partial \bar{W}}{\partial \lambda_\theta}\frac{\partial \lambda_\theta}{\partial s} = -\frac{2v}{s^3}\frac{\partial \bar{W}}{\partial \lambda_r} + 2\frac{\partial \bar{W}}{\partial \lambda_\theta}. \tag{26}$$

The combination of (24), (26) and (20) gives $T_{rr} - T_{\theta\theta} = -(s/2v)\partial w(s,v)/\partial s$ so that the equilibrium equation (16) can be expressed as

$$\frac{dT_{rr}}{dr} = \frac{s}{rv}\frac{\partial w(s,v)}{\partial s}. \tag{27}$$

This is now integrated with the aid of (17) and (23) to yield

$$\Delta P \equiv P_i - P_o = \int_{s_i}^{s_o} \frac{1}{v - s^3}\frac{\partial w(s,v)}{\partial s} ds. \tag{28}$$

Because s_o is determined by s_i from (22) it follows that ΔP from (28) is indeed a function of s_i. In the absence of swelling, meaning that $v = 1$ identically, (28) retrieves a standard expression from conventional incompressible, isotropic hyperelasticity (see (7.18) of Green & Shield (1950) and (5.3.21) of Ogden (1997)). The above swelling generalization is equivalent to that given in (22) of Pence & Tsai (2006).

In general the swelling field v could depend on position within the shell wall, i.e., $v = v(R)$. This would then require v to be treated as a function of s for the purpose of the integration in (28), say $v(R) = \hat{v}(s)$. Such a treatment could be developed but we will not do so in this paper. Instead *we shall henceforth restrict attention to homogeneous swelling in the shell wall. This means that v is constant as a function of R, however such a v could vary with time in a quasi-static fashion.* Thus in this work we now restrict attention to homogeneous swelling where v is a time-dependent parameter. It then follows from (13)

that

$$r = \left(r_i^3 + v(R^3 - R_i^3)\right)^{1/3}. \tag{29}$$

For the case of material model (6), one obtains that

$$w(s,v) = \left(\frac{v^2/s^4 + 2s^2}{v^{2/3}} - 3\right) d_1 + \left(\frac{s^4 + 2v^2/s^2}{v^{4/3}} - 3\right) d_2 \tag{30}$$

and this in turn puts (28) in the form

$$\Delta P = \int_{s_i}^{s_o} \frac{4}{v - s^3}\left[\left(\frac{s}{v^{2/3}} - \frac{v^{4/3}}{s^5}\right) d_1 + \left(\frac{s^3}{v^{4/3}} - \frac{v^{2/3}}{s^3}\right) d_2\right] ds. \tag{31}$$

Note that (31) continues to allow for the possibility of $d_1 = d_1(v)$ and $d_2 = d_2(v)$. Equation (31) in conjunction with

$$s_o = \frac{1}{R_o}\left(R_i^3\ s_i^3 + v(R_o^3 - R_i^3)\right)^{1/3} \tag{32}$$

provides the general relation between: amount of swelling v, applied pressure ΔP, and inner radius expansion $r_i = s_i\ R_i$ for a material with swelling dependent stored energy density (6). Although the integration associated with (31) could certainly be performed, the resulting lengthy analytical expression does not provide much insight. Instead, we obtain results by generalizing ideas put forward by Carroll in the context of the incompressible theory (in which there is no swelling concept).

4. The role of swelling in the pressure-inflation relation

In the absence of swelling, the inflation of a pressurized spherical shell is a classical problem that has been widely studied within the theory of incompressible finite hyperelasticity, i.e., with the constraint $\det\mathbf{F} = 1$. As first discussed in detail by Green and Shield Green & Shield (1950), a radially symmetric spherical inflation is possible in every isotropic homogeneous incompressible hyperelastic material. Ultimately, it is given by the $v = 1$ version of (28) and (30). This permits the construction of an *inflation graph*, which is a plot of ΔP as a function of r_i. A basic discussion on different qualitative forms for the inflation graph is given by Carroll Carroll (1987). This in turn allows one to identify different material classes. As we now show, these concepts readily generalize so as to provide similarily useful organizing concepts when swelling takes place.

4.1. Uniform expansion occurs for homogeneous swelling in the absence of pressure

While the discussion in Carroll (1987) made no reference to the swelling concept, the concept is easily introduced into the treatment. Namely, there is now a separate inflation graph for each value of v. As v is increased continuously, it generates a family of inflation graphs in a continuous fashion. We consider the basic features of this family of graphs for a material obeying the Baker-Ericksen type condition (4). Using (24) this condition, henceforth referred to as the *B-E* condition, becomes

$$(T_{rr} - T_{\theta\theta})(\lambda_r - \lambda_\theta) = \frac{s^3 - v}{2v\,s}\frac{\partial w}{\partial s} = \underbrace{-\frac{(v - s^3)^2}{2vs}}_{\leq 0}\ \underbrace{\frac{1}{v - s^3}\frac{\partial w}{\partial s}}_{\text{integrand of (28)}}. \tag{33}$$

Thus the B-E condition (4) gives that the integrand in (28) is negative at all locations where $\lambda_r \neq \lambda_\theta$. What happens if $\lambda_r = \lambda_\theta$? Isolated locations where λ_r and λ_θ coincide have no effect on the overall integral. This leaves a case in which λ_r and λ_θ coincide on some interval in s. In that case $r' = r/R = v^{1/3}$ on that interval. Then, because $s = r/R = v^{1/3}$ which is a single value, the interval is in fact just a single point. We conclude that (4) ensures that the integrand of (28) is negative except at possible isolated locations that do not effect the evaluation of the integral.

It is useful to remark upon the special case for which $\lambda_r = \lambda_\theta$ for all R within the shell wall. This corresponds to $r' = r/R = v^{1/3}$ for all R, i.e., $r^3 = vR^3$ throughout the spherical shell. This represents a *uniform expansion*. For a uniform expansion it follows that $s = r/R = v^{1/3}$ for all R so that $s_o = s_i = v^{1/3}$. Consequently the limits of integration in (28) are identical and thus $\Delta P = 0$. This gives the baseline result:

- In the absence of pressurization ($\Delta P = 0$), homogeneous swelling causes the sphere to undergo uniform expansion ($r^3 = vR^3$). This gives $\lambda_\theta = \lambda_r$ and $T_{rr} = T_{\theta\theta}$ for all R.

Such a homogeneous swelling expansion is represented by the point $(s_i, \Delta P) = (v^{1/3}, 0)$ on the inflation graph.

Suppose now that $r^3 > vR^3$, i.e., an amount of inflation that exceeds uniform expansion. This will be the case if $r_i > v^{1/3}R_i$. Then $s^3 = r^3/R^3 > v$ and it follows from (23) that $ds/dr < 0$ and hence $s_o < s_i$. Thus the integral in (28), because the integrand is negative, gives $\Delta P > 0$. Furthermore $\lambda_\theta = r/R > v^{1/3}$, $\lambda_r = r' = vR^2/r^2 < v^{1/3}$ and hence $T_{\theta\theta} > T_{rr}$

for all R. Consequently one obtains another useful result, the first part of which is also intuitive:

- A positive pressurization $\Delta P > 0$ causes the inflation to exceed that of the uniform expansion due to the swelling alone. Then $\lambda_r < v^{1/3} < \lambda_\theta$ and $T_{rr} < T_{\theta\theta}$ for all R.

In a similar fashion, it follows that $\Delta P < 0$ gives an inflation that is less than that of a swelling induced uniform expansion. In such a case one might also expect various wrinkling type instabilities that break the spherical symmetry. For this reason we restrict attention to $\Delta P \geq 0$. For the same reason we also avoid the consideration of de-swelling ($0 < v < 1$).

4.2. Qualitative behavior in the absence of swelling

For a specified value of v the form of the pressure-inflation graph is determined by the stored energy density W using (28). The resulting relation between ΔP and $s_i = r_i/R_i$ is dependent on the shell thickness. This shell thickness will be characterized by the thickness ratio parameter

$$\xi \stackrel{\text{def}}{=} R_i/R_o, \qquad 0 < \xi < 1. \tag{34}$$

The *thin shell limit* is then $\xi \to 1$. The other limit of $\xi \to 0$ can be viewed either as a microvoid in a finite body or as a spherical hole in an infinite body.

If $v = 1$, i.e. no swelling at all, then we are in the domain of conventional incompressible hyperelasticity and the problem reduces to one that has been extensively studied. In this conventional incompressible hyperelastic context, Carroll Carroll (1987) identifies three different types of behavior which he names type (a), type (b) and type (c). These three types are diagrammed in Figure 1 and are described as follows:

- type (a) behavior: ΔP increases monotonically with increasing r_i;
- type (b) behavior: ΔP increases to a maximum value and then decreases to a nonnegative asymptotic value;
- type (c) behavior: ΔP first increases to a local maximum, then decreases to a local positive minimum before again monotonically increasing.

In the hyperelastic theory without swelling, certain stored energy forms W always give an inflation graph with type (a) behavior. The Mooney-Rivlin material (5) specialized to $d_1 = 0$ and $d_2 > 0$ is such a material.

Other stored energy forms always give an inflation graph with type (b) behavior; the neo-Hookean material, meaning a Mooney-Rivlin material (5) with $d_2 = 0$ and $d_1 > 0$, is such a material.

Finally there are certain stored energy forms that give type (a) behavior if ξ is relatively small but give type (c) behavior if ξ is relatively large (close to one). The Mooney-Rivlin material (5) with $d_1 = 10d_2$ is such a material. For these materials there is a transitional value of the thickness ratio $R_i/R_o = \xi$, say $\xi_{a/c}$, such that $\xi < \xi_{a/c}$ implies type (a) behavior and $\xi > \xi_{a/c}$ implies type (c) behavior. Alternatively stated, these materials have a type (c) inflation graph for thin shell geometries but have a type (a) inflation graph for thick shell geometries. While the above classification framework was established by Carroll Carroll (1987) for the incompressible theory ($v \equiv 1$) we now use it to describe the swelling materials under consideration.

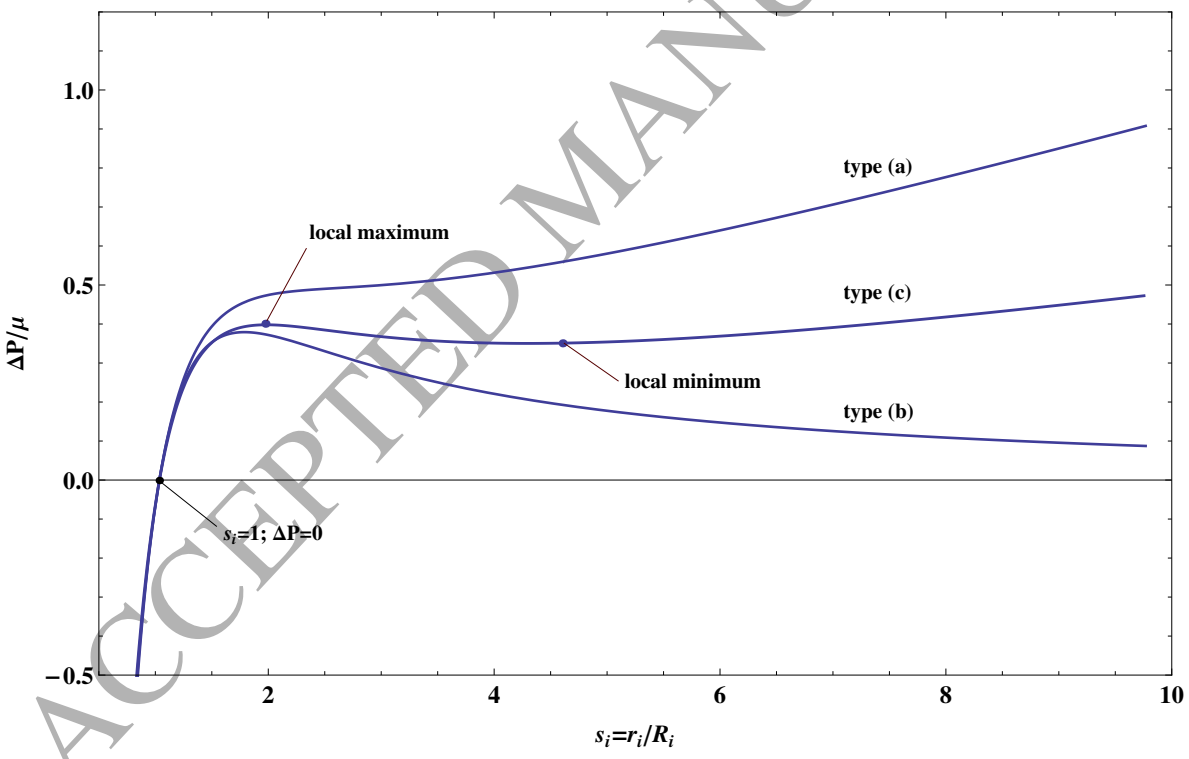

Figure 1: Inflation graphs showing three qualitatively different types of behavior (a)-(c) in the absence of swelling. These particular graphs correspond to W given by (5), all with thickness ratio $\xi = 0.5$. The differences are due to the values of d_1 and d_2. Here: $d_1 = 4d_2$ (top); $d_1 = 9d_2$ (middle); and $d_2 = 0$ (bottom).

4.3. Quantitative Determination of the Inflation Behavior Type

For any fixed value $v > 1$ the inflation graph will continue to display one of the various behaviors shown in Figure 1. However changes in v could cause a transition from one behavior type to another. For this reason it is useful to obtain a more quantitative characterization of the conditions that distinguish the different graph behaviors. The presence of either a local maximum or a local minimum in the inflation graph is dependent on whether the derivative $\dfrac{d}{ds_i}(\Delta P)$ vanishes for some value of s_i. It follows from (28) that this derivative is given by

$$\frac{d}{ds_i}(\Delta P) = \frac{s_i^2}{v - s_i^3}\left(\frac{1}{s_o^2}\frac{\partial w}{\partial s}\bigg|_{s_o} - \frac{1}{s_i^2}\frac{\partial w}{\partial s}\bigg|_{s_i}\right), \tag{35}$$

where use has been made of (13) and the connections

$$s_o^3 = s_i^3\xi^3 + v(1-\xi^3), \qquad \frac{ds_o}{ds_i} = \xi^3\frac{s_i^2}{s_o^2}. \tag{36}$$

Equation (35) shows that the inflation graph will have a zero slope location only if the following condition is met:

$$\frac{d}{ds_i}(\Delta P) = 0 \qquad \Leftrightarrow \qquad \frac{1}{s_o^2}\frac{\partial w}{\partial s}\bigg|_{s_o} = \frac{1}{s_i^2}\frac{\partial w}{\partial s}\bigg|_{s_i}. \tag{37}$$

To make use of this condition let η be the similarity variable v/s^3. Because we restrict attention to $\Delta P \geq 0$ it then follows that $r \geq v^{1/3}R$ and hence

$$0 < \eta = v/s^3 \leq 1. \tag{38}$$

Next define the auxiliary function

$$G(\eta, v) \stackrel{\text{def}}{=} \tfrac{1}{2}v^{1/3}\eta^{2/3}\frac{\partial w(s,v)}{\partial s}\bigg|_{s=(\eta/v)^{-1/3}}. \tag{39}$$

Using (39) it follows that condition (37) is equivalently expressed as

$$\frac{d}{ds_i}(\Delta P) = 0 \qquad \Leftrightarrow \qquad G(\eta_i, v) = G(\eta_o, v), \tag{40}$$

with

$$\eta_i = v/s_i^3, \qquad \eta_o = v/s_o^3. \tag{41}$$

Conditions (20), (26) and (39) enable a physical interpretation for the function G in terms of swelling v, stretch $s = \lambda_\theta$, and stresses $T_{\theta\theta}, T_{rr}$, namely

$$G(\eta, v)\Big|_{\eta = vR^3/r^3} = \frac{v^2}{\lambda_\theta^3}(T_{\theta\theta} - T_{rr}). \tag{42}$$

Now for any fixed value v, the development in Section 4.2 showed that a uniform expansion takes place if $\Delta P = 0$. This means that $s = r/R = v^{1/3}$ for all R so that, in particular, $s_o = s_i = v^{1/3}$ and hence $\eta_i = \eta_o = 1$. Because all of the principle stretches are then coincident one also obtains from (20) that $T_{\theta\theta} = T_{rr}$. Consequently (42) indicates that

$$G(1, v) = 0. \tag{43}$$

Conversely, $\Delta P > 0$ gives $s_i > s_o > v^{1/3}$ which in turn implies $s_i^3 > s_o^3 > v$ and hence $0 < v/s_i^3 < v/s_o^3 < 1$. It follows that the first arguments of G in (40) are ordered

$$0 < \eta_i < \eta_o < 1 \quad \text{when} \quad \Delta P > 0. \tag{44}$$

Also in this case the B-E inequality (4) gives $T_{\theta\theta} > 0 > T_{rr}$ at each location R of the nonuniform spherical expansion. Hence (42) yields

$$G(\eta, v) > 0 \quad \text{for } 0 < \eta < 1. \tag{45}$$

Figure 2 shows graphs for $G(\eta, v)$ corresponding to each of the three inflation curves displayed in Figure 1 computed on the basis of (39) taking $v = 1$. The three graphs are ordered from top to bottom in the same way as the graphs in Figure 1. Note that each of the three graphs in Fig. 2 obey both of the conditions (43) and (45). The two top curves tend to ∞ as $\eta \to 0$ while the bottom curve goes to zero at $\eta = 0$. The top curve is monotone decreasing, the middle curve is decreasing-increasing-decreasing, and the bottom curve is increasing-decreasing. As we discuss next, these behaviors correlate with the type (a), type (c) and type (b) behaviors exhibited in Figure 1.

To make direct contact with condition (40) we define the function that maps η_i to η_o for the specific thickness ratio ξ under consideration. In view of (36) this function is

$$\hat{\eta}_o(\eta_i, \xi) \stackrel{\text{def}}{=} \frac{\eta_i}{\xi^3 + \eta_i(1 - \xi^3)}. \tag{46}$$

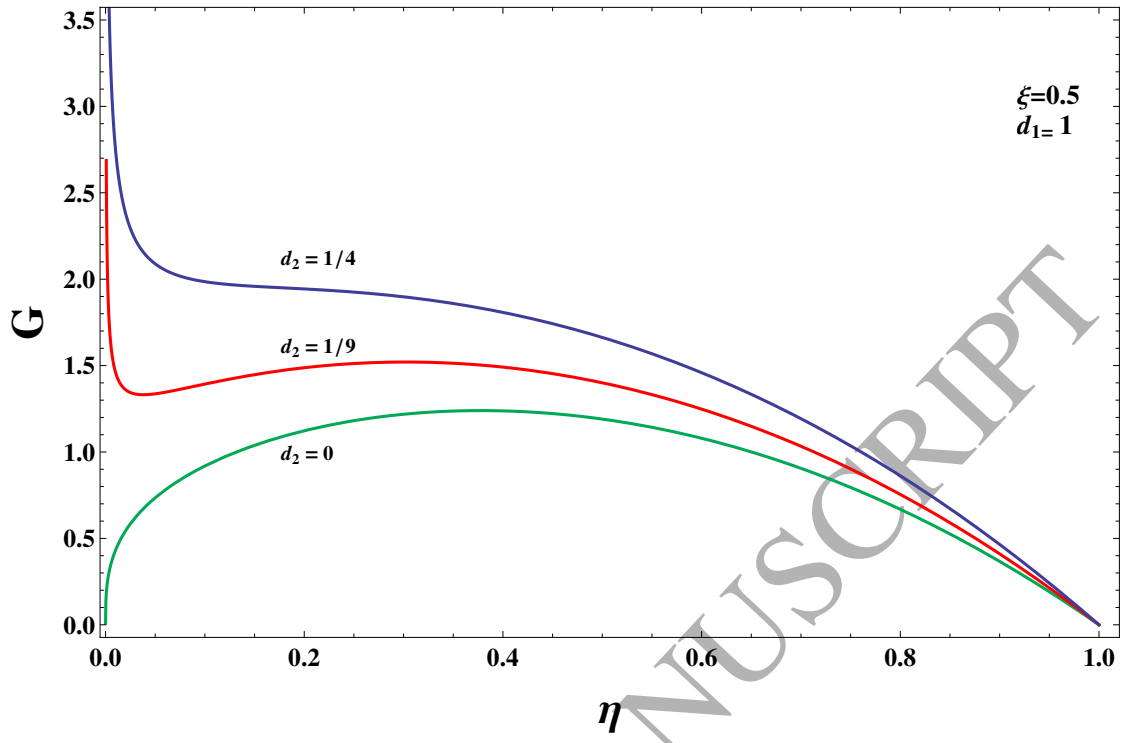

Figure 2: Graphs for $G(\eta, v)$ corresponding to the three inflation curves in Figure 1. The function $G(\eta, v)$ is computed on the basis of (39) using (6) and taking $v = 1$. This is equivalent to using (5) and ultimately gives the expression (50) that we examine in more detail later.

The function $\hat{\eta}_o$ is now used to define the composite function $H \stackrel{\text{def}}{=} \{G \circ \hat{\eta}_o\}$, i.e.,

$$H(\eta, v, \xi) \stackrel{\text{def}}{=} G\big(\hat{\eta}_o(\eta, \xi), v\big). \tag{47}$$

We now have two functions: $G(\eta, v)$ defined in (39) and $H(\eta, v, \xi)$ defined in (47). In general these are different functions of their first argument η. An exception occurs when $\xi = 1$. This is because (46) gives $\hat{\eta}_o(\eta_i, 1) = \eta_i$ which in turn provides $G(\eta_i, v) = H(\eta_i, v, 1)$.

The stationary value characterization (40) is now expressed as

$$\frac{d}{ds_i}(\Delta P) = 0 \qquad \Leftrightarrow \qquad G(\eta_i, v) = H(\eta_i, v, \xi). \tag{48}$$

We seek to determine under what circumstances, namely for what values (η_i, v, ξ), the condition (48) is met. For this reason we now, for the rest of this section, use η_i for the first argument of both G and H. The previous result (45) establishes that $G(\eta_i, v)$ is a strictly positive function of η_i on $0 < \eta_i < 1$. The function $H(\eta_i, v, \xi)$ is similarly strictly positive

on $0 < \eta_i < 1$. Also (43) gives that $H(1, v, \xi) = G(1, v) = 0$.

Fix the value v and consider the graphs of $G(\eta_i, v)$ and $H(\eta_i, v, \xi)$ as a function of η_i on the interval $0 < \eta_i \leq 1$ for different values of ξ. Because $G(1, v) = H(1, v, \xi) = 0$ these graphs meet at the endpoint $\eta_i = 1$. However because of inequality (44):

> *The graph of H is shifted to the left of the graph of G on the interval $0 < \eta_i < 1$. The amount of this shift is nonuniform in η_i and is dependent upon ξ.*

In the thin shell limit $\xi \to 1$ this shift becomes vanishingly small. Figure 3 shows such a leftward shift for each of the three G graphs from Figure 2. In particular, each of the Fig. 2 graphs is redisplayed as solid curve. The left shifted graphs are displayed as dashed curves of the same color. We take $\xi = 0.5$ because this gives the thickness ratio associated with the curves from Figure 1. Because $\xi = 0.5$ is not close to one (i.e., the shell is thick) the amount of leftward shift is large and this causes the H curves to become distorted relative to the original G curves. However, what is not changed for each same color pair is the monotonicity properties: decreasing for the blue pair, decreasing-increasing-decreasing for the red pair, increasing-decreasing for the green pair. In other words the monotonicity properties of H as a function of η_i do not vary with ξ and so can be regarded as inherited from the original function G.

Condition (48) holds if and only if the graph of G intersects the graph of H somewhere on the interval $0 < \eta_i < 1$. If such an intersection occurs, then the associated value of η_i locates either a maximum or a minimum in the corresponding inflation graph. We now consider the consequences of this observation for each of the three different forms of G shown in Figure 2:

The first and simplest G graph form is one that is monotonically decreasing as a function of η_i. In this case the graph of G cannot intersect its shifted image H. Consequently,

- forms for W that generate a monotonically decreasing G as a function of η_i always give a type (a) inflation graph.

This case is represented by the pair of blue curves in Figure 3. The solid and dashed blue curves do not intersect, and consequently the corresponding inflation graph in Figure 1 is monotone.

The second graph form for G is one in which it is decreasing-increasing-decreasing as a function of η_i as represented by the red curve of Figure 2. It then follows that a small shift

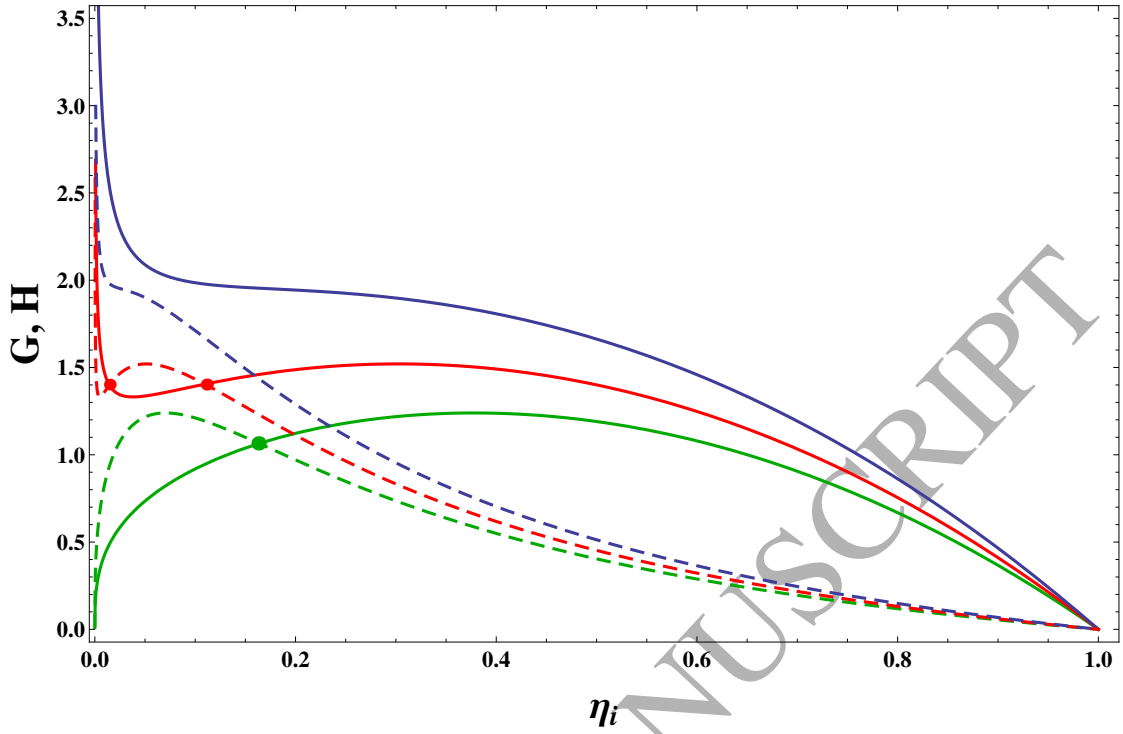

Figure 3: G graphs from Fig. 2 (solid) along with the corresponding H graphs (dashed) for thickness ratio $\xi = 0.5$. Each point on a G graph is shifted to the left to give a corresponding point on the H graph. This shift is small if ξ is close to one (a thin shell). Here, because ξ is not very close to one, the nonuniform shift distorts the curves, however the basic monotonicity properties do not change.

to the left of this graph will result in two intersections of the original graph with its shifted image. The associated inflation graph will then have a local maximum followed by a local minimum, in other words type (c) behavior. In this graphical construction the amount of shift increases as ξ decreases from $\xi = 1$, i.e., as the shell gets thicker. This is represented by the pair of red curves in Figure 3. There are two points of intersection, and these correspond to the local maximum and local minimum of the middle curve in Figure 1.

Eventually however, the amount of shift will be sufficient to cause the shifted graph to clear itself of any intersection with the original graph. The specific shift associated with just losing this intersection involves the two intersection points coming together at a single special intersection point where the two graphs now have a common tangent. At this special shift, not only does (48) hold, but also

$$\frac{\partial}{\partial \eta_i} G(\eta_i, v) = \frac{\partial}{\partial \eta_i} H(\eta_i, v, \xi). \tag{49}$$

This now becomes an equation for the value of ξ associated with a transition from type (c) behavior to type (a) behavior. Consequently:

- forms for W that generate a G function that is decreasing-increasing-decreasing on $0 < \eta_i < 1$ give type (c) inflation behavior for thin shells and type (a) inflation behavior for thick shells. The special transition value $\xi = \xi_{a/c}$ is found by simultaneous solution of (48) and (49) for η_i and ξ.

The third and final graph form for G is one that obeys $G = 0$ at $\eta_i = 0$ and which then increases with η_i before decreasing back to zero at $\eta_i = 1$. In this case all left shifted curves for H will have exactly one intersection with the original G curve. Hence there will be a type (b) inflation graph for all values of ξ. Consequently:

- forms for W that generate a G function that is increasing-decreasing on $0 < \eta_i < 1$ always give a type (b) inflation graph.

It is important to realize that the above inflation graph characterization in terms of G has focused on the effect of η_i and ξ irrespective of the value of v. In other words the homogeneous swelling value v has been regarded as a fixed parameter in all of the above discussion. However, for a given stored energy density $W(I_1, I_2, v)$ the conclusions based on the above G graph treatment for one value of v could differ from the conclusions obtained for a different value of v. For example, the graph of G could be monotonically decreasing with η_i for values of v at and near $v = 1$, but could be decreasing-increasing-decreasing for relatively larger values of v. In such a case, if the shell is sufficiently thin, such a W would lead to a type (a) inflation graph when the material is unswollen but would give a type (c) inflation graph when the material is swollen. It is this issue of swelling induced changes in qualitative behavior to which we now turn our attention.

5. The swellable Mooney-Rivlin material

We illustrate the effect of a changing amount of swelling using the material constitutive law (6). Thus for $v = 1$ this retrieves the familiar Mooney-Rivlin form (5).

5.1. Inflation behavior prior to swelling

Setting $v = 1$ in $G(\eta, v)$ gives a function that shall be denoted by $g(\eta)$, i.e., $g(\eta) \stackrel{\text{def}}{=} G(\eta, 1)$. This removes v from consideration and effectively reduces the analysis procedure to that described by Carroll Carroll (1987) for conventional incompressible isotropic hyperelastic materials (i.e., no volume change). For the conventional Mooney-Rivlin material (5) this function is given by

$$g(\eta) = 2d_1(\eta^{1/3} - \eta^{7/3}) + 2d_2(\eta^{-1/3} - \eta^{5/3}). \tag{50}$$

Note that $g(1) = 0$. Also $g(\eta) \to \infty$ as $\eta \to 0$ provided that $d_2 > 0$. However if $d_2 = 0$ then $g(0) = 0$. Indeed the cases used in generating the graphs in Figures 1 - 3 all corresponded to this specific example.

By considering the equivalent of the derivative of g, Carroll Carroll (1987) shows how the monotonicity of this g is dependent upon the parameter ratio d_2/d_1. In particular, the following critical value

$$(d_2/d_1)|_{cr} \stackrel{\text{def}}{=} \max_{0<\eta<1} \left[\frac{\eta^{-2/3} - 7\eta^{4/3}}{5\eta^{2/3} + \eta^{-4/3}} \right] \approx 0.215 \tag{51}$$

has special significance. Carroll shows that if d_2/d_1 is greater than this critical value then $g(\eta)$ is monotone decreasing on $0 < \eta \leq 1$, but if d_2/d_1 is less than this critical value then $g(\eta)$ is decreasing-increasing-decreasing.

For our purposes it is convenient to examine the resulting consequences after expressing d_1 and d_2 in the form

$$d_1 = \tfrac{1}{2}\alpha\mu, \qquad d_2 = \tfrac{1}{2}(1-\alpha)\mu \tag{52}$$

which in turn gives

$$\frac{d_2}{d_1} = \frac{1-\alpha}{\alpha}, \qquad \alpha = \frac{d_1}{d_1 + d_2}. \tag{53}$$

The reason for introducing (52) and (53) is that it makes $\mu > 0$ the shear modulus. Indeed using (52) in (5) gives an alternative standard way of writing the Mooney-Rivlin energy form. The parameter α is in the interval $0 \leq \alpha \leq 1$. The special ratio of d_2/d_1 given in (51) corresponds to the critical value

$$\alpha_{cr} = \left. \frac{d_1}{d_1 + d_2} \right|_{cr} = \left. \frac{1}{1 + (d_2/d_1)} \right|_{cr} \approx 0.823. \tag{54}$$

The derivative $dg/d\eta = g^{'}(\eta)$ that is computed from (50) has two roots if α is in the range $\alpha_{cr} < \alpha < 1$ and has no roots if α is in the range $0 \leq \alpha < \alpha_{cr}$. This identifies the behavior of the inflation graph as follows:

- If $0 \leq \alpha < \alpha_{cr}$ then the function g is monotonically decreasing with η. The inflation graph has no stationary value and so gives type (a) behavior for all ξ.
- If $\alpha_{cr} < \alpha < 1$ then the function g is decreasing-increasing-decreasing. The behavior is either type (a) or type (c) depending on whether ξ is greater or less than a transitional value $\xi_{a/c} = \xi_{a/c}(\alpha)$. If $\xi > \xi_{a/c}$ then the behavior is type (c). If $\xi < \xi_{a/c}$ then the behavior is type (a).
- If $\alpha = 1$ then $d_2 = 0$ and $g(0) = 0$. This is the neo-Hookean special case and the function g has only one stationary value. The behavior is then type (b) for all ξ.

As described in the discussion following (49), the transition value of ξ when $\alpha_{cr} < \alpha < 1$ can be obtained by simultaneous solution of (48) and (49). This gives a value $\xi_{a/c} = \xi_{a/c}(\alpha)$ for each value of α in the range $\alpha_{cr} < \alpha < 1$ when $v = 1$. The curve $\xi = \xi_{a/c}(\alpha)$ is plotted in Figure 4. Any ordered pair (ξ,α) that is above the curve $\xi = \xi_{a/c}$ corresponds to a structure (characterized by ξ) composed of a material (characterized by α) that gives an inflation graph having type (c) behavior. Conversely, ordered pairs (ξ,α) below the curve $\xi = \xi_{a/c}$ correspond to a structure-material combination with a type (a) inflation graph. All of this follows directly from Carroll's work Carroll (1987).

5.2. Inflation graph sequences for increasing swelling

When swelling is present we consider the generalization of (5) that is given by (6). Then g as given by (50) generalizes to

$$G(\eta, v) = 2(\eta^{1/3} - \eta^{7/3})d_1(v) + 2(\eta^{-1/3} - \eta^{5/3})d_2(v). \tag{55}$$

The direct correspondence between (55) and (50) is due to the scalings $I_1/v^{2/3}$ and $I_2/v^{4/3}$ in (6). This allows the analysis of G in (55) to proceed in a similar fashion to the previous analysis of (50). The main difference is that now we must account for the possible dependence of the ratio d_2/d_1 upon v.

We begin by considering the case where d_1 and d_2 are independent of v. According to (53) this is equivalent to α being independent of v. In this case homogeneous swelling has no

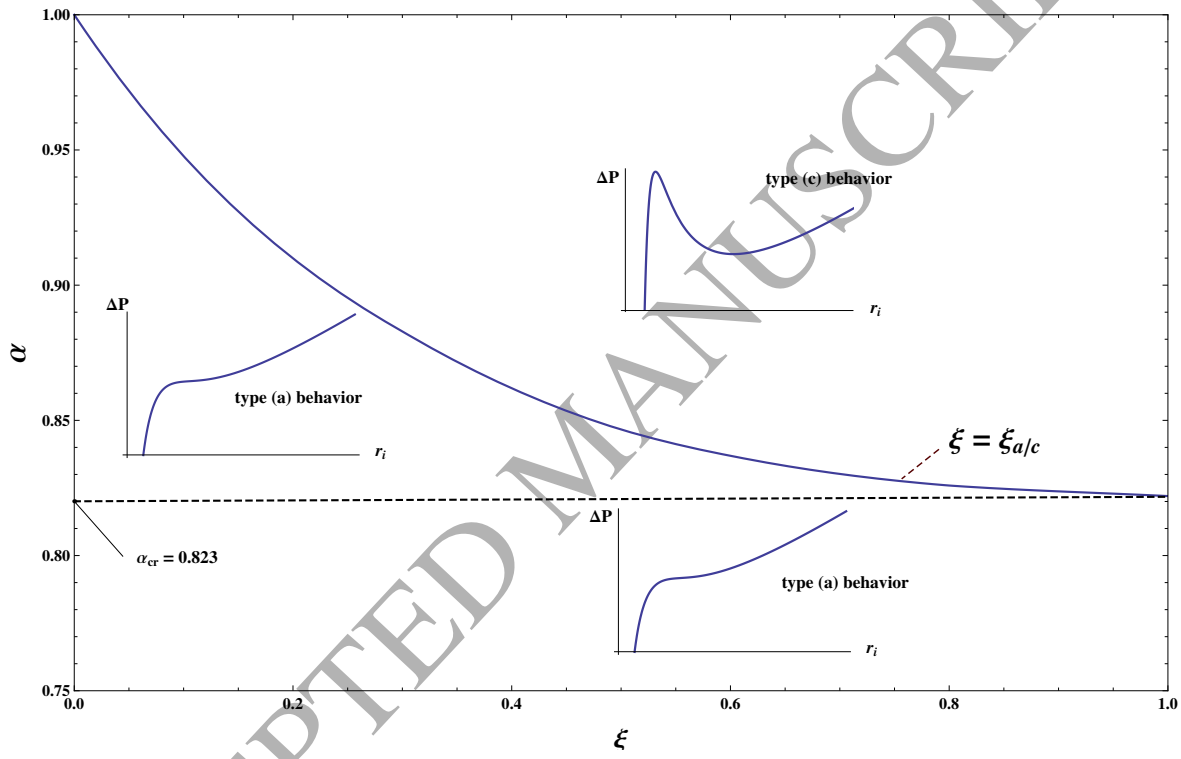

Figure 4: Qualitative behavior of the inflation graph for the Mooney-Rivlin model $W = d_1(I_1 - 3) + d_2(I_2 - 3)$ as a function of material parameter $\alpha = d_1/(d_1 + d_2)$ and thickness ratio $\xi = R_i/R_o$. The curve $\xi = \xi_{a/c}$ provides a transition between type (c) and type (a)-behavior.

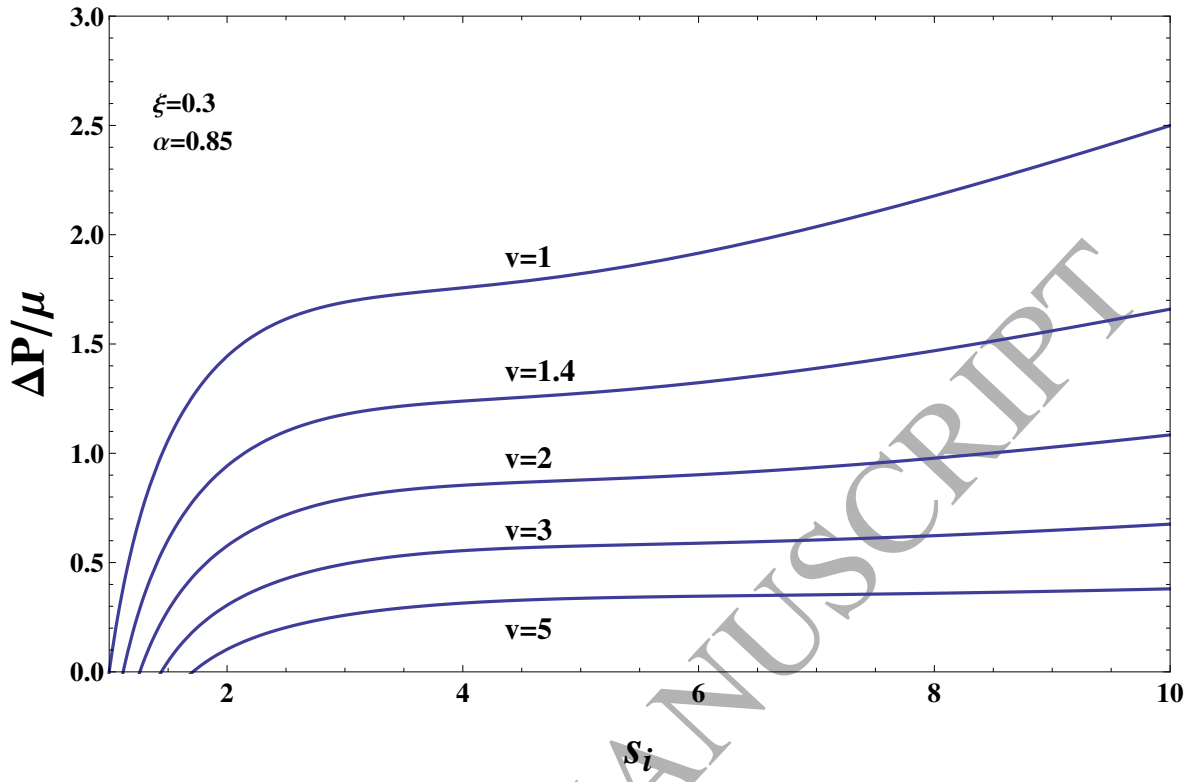

Figure 5: Inflation graphs for the Mooney-Rivlin-type model (6) using (52) with $\alpha = 0.85$, and thickness ratio $\xi = R_i/R_o = 0.3$. All the inflation graphs exhibit type (a) behavior.

effect on the type of inflation graph. Such a result is consistent with remarks given in Pence & Tsai (2006). As a first example, consider the material parameter $\alpha = 0.85$. Then, because $\alpha = 0.85 > \alpha_{cr}$, there is a transition value of $\xi_{a/c}$ which, according to Figure 4, is given by $\xi_{a/c} = 0.47$. We now separately consider $\xi = 0.3 < \xi_{a/c}$ (a relatively thick walled structure) and $\xi = 0.7 > \xi_{a/c}$ (a relatively thin walled structure). The pair $(\xi, \alpha) = (0.3, 0.85)$ is in the type (a) behavior region of Figure 4, and so the $v = 1$ inflation graph for $\xi = 0.3$ displays type (a) behavior. This inflation graph is shown in Figure 5 along with the inflation graphs for an increasing sequence of v values. Because d_2/d_1 is independent of v all of the inflation graphs are monotonic. Turning to the pair $(\xi, \alpha) = (0.7, 0.85)$, which is in the type (c) behavior region of Figure 4, it follows that the $v = 1$ inflation graph for $\xi = 0.7$ displays type (c) behavior. Figure 6 shows this inflation graph along with those for a similarly increasing sequence of swelling values v. Because d_2/d_1 is again independent of v all of these graphs exhibit type (c) behavior.

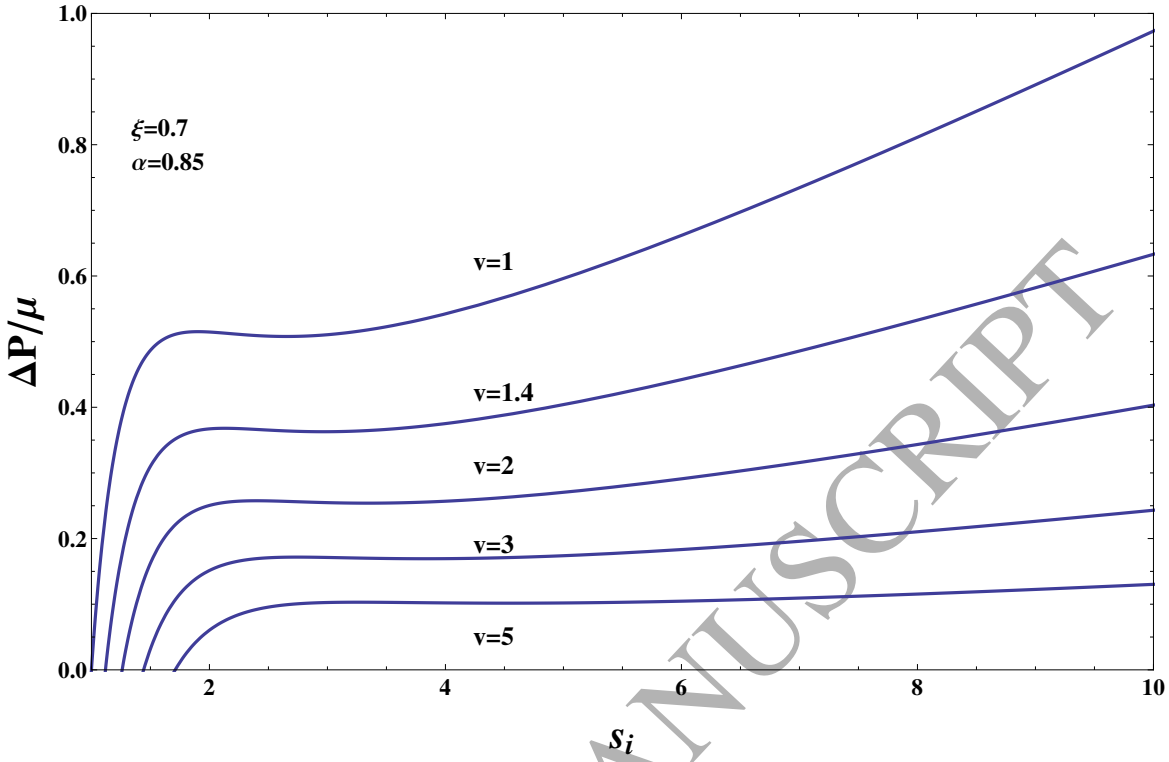

Figure 6: Inflation graphs for the same material as in Fig. 5 (i.e., (6) and (52) with $\alpha = 0.85$), but now the thickness ratio $\xi = 0.7$. This corresponds to a relatively thinner walled structure. All the inflation graphs now exhibit type (c) behavior.

5.3. Swelling dependent material stiffness parameters

More generally the parameters d_1 and d_2 may be swelling dependent, i.e., $d_1 = d_1(v)$ and $d_2 = d_2(v)$. It then follows that the ratio $d_1(v)/d_2(v)$ changes with the amount of swelling. This can lead to the inflation graph behavior changing its type as v increases. To demonstrate consider materials for which the Mooney-Rivlin parameters $d_1(v)$ and $d_2(v)$ in (6) have the form

$$d_1 = \tfrac{1}{2}\mu\alpha\, v^p \quad \text{and} \quad d_2 = \tfrac{1}{2}\mu(1-\alpha)\, v^q, \tag{56}$$

where $\mu > 0$ and $0 \le \alpha \le 1$ are fixed material constants. This is consistent with (52) as can be seen by taking $v = 1$. Equation (56) introduces the additional exponent parameters p and q. The choice $p = 0$ and $q = 0$ then formally retrieves the case that was just examined in Section 5.2 with both d_1 and d_2 independent of v.

For $p \neq 0$ and $q \neq 0$ the material behavior remains dependent on the ratio

$$\frac{d_2}{d_1} = \frac{1-\alpha}{\alpha} v^{q-p}. \tag{57}$$

Thus if $p = q$ then the ratio d_2/d_1 is independent of v and the inflation graph behavior does not change with v. However if $p \neq q$ then the behavior of the function G, which is now determined by d_2/d_1, depends on the amount of swelling v.

The critical value of $(d_2/d_1)_{cr} = 0.215$ from (51) continues to distinguish between monotonic and non-monotonic graphs G. In this regard, for any fixed material parameter α, one may solve (57) for the special swelling value v that is associated with $(d_2/d_1)_{cr}$. Define this special value of v as $v_{A\leftrightarrow C}$. Making the replacements $d_2/d_1 \to (d_2/d_1)_{cr}$ and $v \to v_{A\leftrightarrow C}$ in (57) and solving for $v_{A\leftrightarrow C}$ yields $v_{A\leftrightarrow C} = v_{A\leftrightarrow C}(p-q,\alpha)$ with

$$v_{A\leftrightarrow C}(p-q,\alpha) \stackrel{\text{def}}{=} \left(\frac{\alpha}{1-\alpha}\,(d_2/d_1)_{cr}\right)^{\frac{1}{q-p}} = (0.215)^{\frac{1}{q-p}} \big(\frac{\alpha}{1-\alpha}\big)^{\frac{1}{q-p}}. \tag{58}$$

Now working through the various possibilities it follows that:

$$\text{if } p < q \text{ then the graph of } G \text{ is} \begin{cases} \text{monotone whenever} & v > v_{A\leftrightarrow C}, \\ \text{non-monotone whenever} & v < v_{A\leftrightarrow C}, \end{cases} \tag{59}$$

and:

$$\text{if } p > q \text{ then the graph of } G \text{ is} \begin{cases} \text{monotone whenever} & v < v_{A\leftrightarrow C}, \\ \text{non-monotone whenever} & v > v_{A\leftrightarrow C}. \end{cases} \tag{60}$$

For the case of a non-monotone G graph, as discussed in Sections 4.2 and 5.1, there is a special value $\xi_{a/c}$ of the thickness ratio ξ that gives the transition between type (a) and type (c) behavior. It is obtained by solving simultaneously the two equations (48) and (49). For given α, p and q, this value is a function of the swelling amount, hence we can write $\xi_{a/c} = \xi_{a/c}(v)$. Such a function is directly useful if one seeks to determine the effect of a fixed amount of swelling as applied to a range of different structures, each with a different shell thickness.

However the more practical problem involves a fixed structure that is subject to a changing

amount of swelling. This motivates an inverting of the relation $\xi = \xi_{a/c}(v)$ to obtain $v = v_{a/c}(\xi)$. The value of swelling $v_{a/c} = v_{a/c}(\xi)$ demarcates the transition between type (a) behavior and type (c) behavior for the given shell geometry. From the material perspective, $v_{a/c}(\xi)$ will depend on α, p and q. In fact, like $v_{A\leftrightarrow C}$ as given in (58), the dependence of $v_{a/c}$ upon p and q will be in terms of $p-q$, i.e., $v_{a/c} = v_{a/c}(\xi, p-q, \alpha)$. However, unlike $v_{A\leftrightarrow C}$ which is independent of ξ and given by the simple form (58), the function $v_{a/c}$ is dependent upon ξ and not given by a similarly simple expression. In fact the connection between these two is that

$$v_{a/c}(\xi, p-q, \alpha)\Big|_{\xi=1} = v_{A\leftrightarrow C}(p-q, \alpha). \tag{61}$$

The qualitative form of the curves $v_{a/c}$ as a function of ξ depends on whether $p > q$ or $p < q$. This is thoroughly discussed in Appendix A. In particular, this appendix explains why (61) holds, and how this leads to the conclusions (59) and (60). This allows a detailed accounting for how the inflation graph varies with v beginning from the originally unswollen value $v = 1$ and then predicting if and when the inflation graph changes its behavior type as v increases.

This can be illustrated by considering the same α and ξ values associated with Figures 5 and 6 but now allowing for $p \neq 0$ and $q \neq 0$. For this purpose we first consider the case $p < q$ that is obtained by taking $p = 0$ and $q = 2/3$. In particular, consider two subcases corresponding respectively to a thick shell ($\xi = 0.3$) and to a relatively thinner shell ($\xi = 0.7$). Thus the two subcases correspond to $(\xi, \alpha, p, q) = (0.3, 0.85, 0, 2/3)$ and to $(\xi, \alpha, p, q) = (0.7, 0.85, 0, 2/3)$. The $v = 1$ curve for the first subcase is identical to the $v = 1$ type (a) curve from Figure 5. Similarly, the $v = 1$ curve in the second subcase matches the $v = 1$ type (c) curve from Figure 6. However the curves for $v > 1$ will no longer match the curves shown in these respective figures. One finds for the first subcase, that with $\xi = 0.3$, the type (a) inflation graph that is present for $v = 1$ persists for all increasing v. This aspect mirrors the situation in Figure 5 even though the individual curves for $v > 1$ are different. In the second subcase of $\xi = 0.7$ one finds that the inflation graph is originally type (c) for $v = 1$ but it eventually transitions to type (a) behavior as v increases. This transition occurs at $v = 1.27$, a result that can be predicted on the basis of the procedure for determining $v_{a/c}$ that is described in the appendix.

The case $p > q$ can be handled similarly. For this purpose consider $p = 2/3$ and $q = 0$, again for the respective thick and thin shell values $\xi = 0.3$ and $\xi = 0.7$. Once again the

$v = 1$ curves match the $v = 1$ curves from Figures 5 and 6 respectively. Once again the $v > 1$ curves do not match the curves in these two figures. In fact, Figures 7 and 8 show a $v > 1$ curve sequence for these two respective cases. For the subcase of $\xi = 0.7$ one finds that the original type (c) behavior at $v = 1$ will persist as v increases (Fig. 8). In contrast, for the case of $\xi = 0.3$ one finds that the original type (a) behavior at $v = 1$ will transition to type (c) behavior as v increases (Fig. 7). This transition occurs at $v = 1.54$, where, again, such a result can be understood in detail on the basis of the treatment given in the appendix.

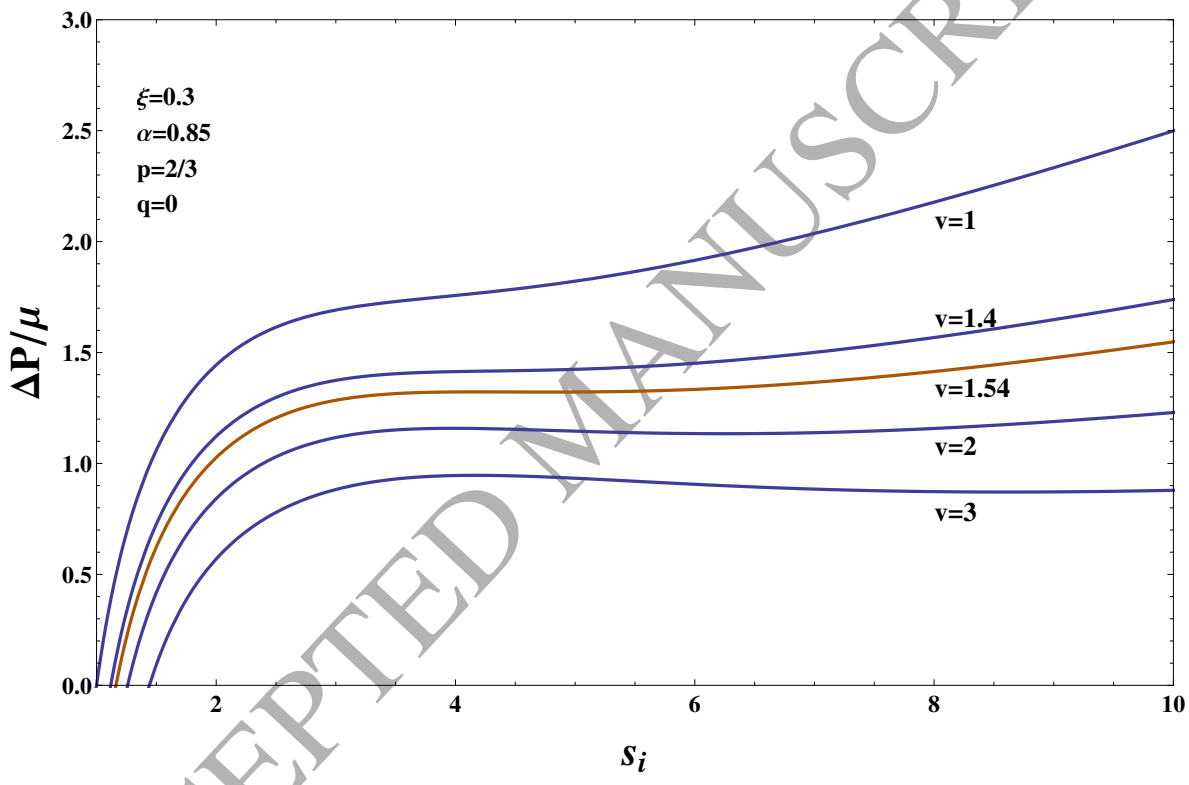

Figure 7: Inflation graphs for the Mooney-Rivlin-type model (6) using (56) with $\alpha = 0.85, p = 2/3, q = 0$, and thickness ratio $\xi = 0.3$. The inflation graphs exhibit the type (a) behavior for $1 \leq v < 1.54$ and type (c) behavior for $v > 1.54$.

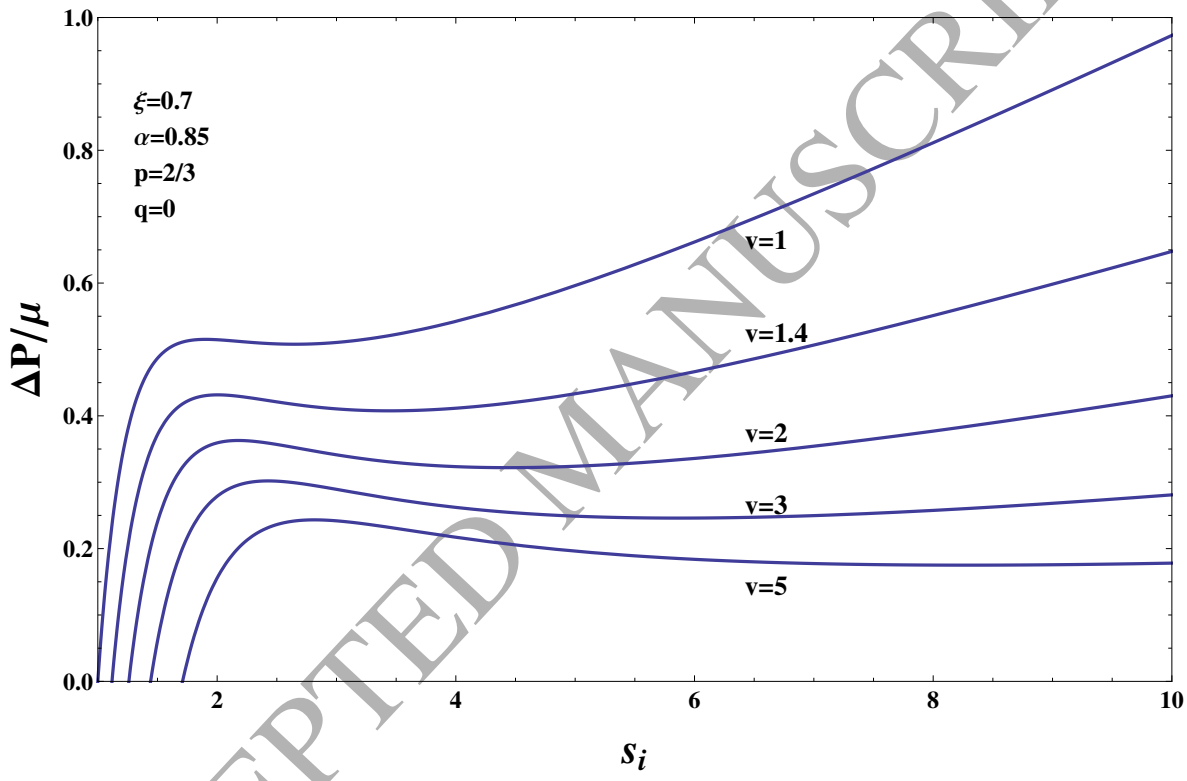

Figure 8: Inflation graphs for the Mooney-Rivlin-type model (6) using (56) with $\alpha = 0.85, p = 2/3, q = 0$, and thickness ratio $\xi = 0.7$. The inflation graphs exhibit type (c) behavior for all $v \geq 1$.

6. Swelling induced burst

Each of the previous Figures 5 - 8 shows a sequence of inflation graphs for a given shell thickness ratio ξ composed of a given model material (α, p, q). Such a figure can be used to gauge how the sphere expands as a function of increasing swelling v. If the pressurization is fixed during the swelling, then a quasi-static increase in v corresponds to moving between different curves on the same figure along the horizontal line determined by the stipulated ΔP. For continuously increasing v the associated increase in s_i will also be continuous so long as all of the curves in the sequence are monotonically increasing. However if the curves are not all monotone increasing then there is clearly the possibility of a discontinuity in s_i.

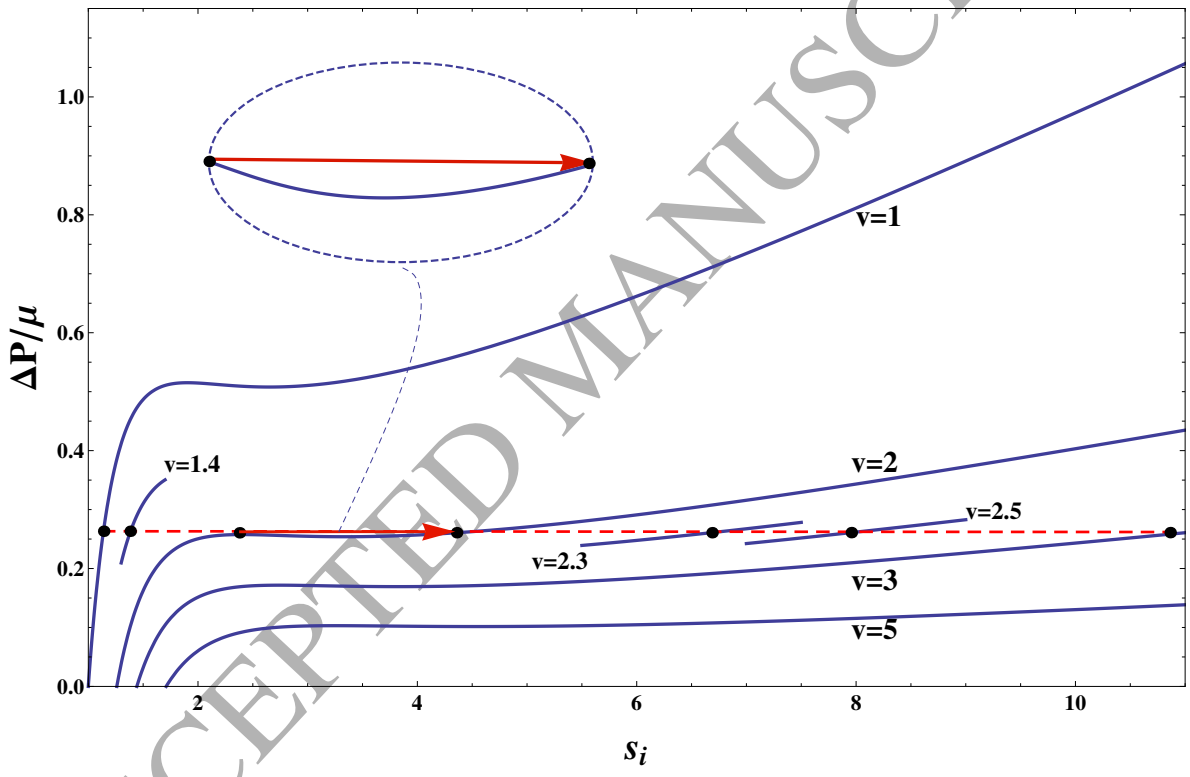

Figure 9: Inflation burst caused by increasing v at fixed $\Delta P = 0.258\mu$ for the inflation graphs from Fig. 6. Prior to swelling the pressurization $\Delta P = 0.258\mu$ has given a mild radial increase (from $s_i = r_i/R_i = 1$ to $s_i = r_i/R_i = 1.14$ on the $v = 1$ curve). Now increasing v at this fixed ΔP gives a continuous increase of s_i with v (dashed red line) until encountering the inflation graph for $v = 2$ where there is a local maximum. Further increase of v requires a jump across to the other increasing branch of the $v = 2$ curve (solid red segment). This corresponds to an inflation burst with radial increase from $s_i = 2.37$ to $s_i = 4.32$.

For example, consider again Figure 6. The inflation graphs for all v are non-monotone (type (c)) and the s_i interval of graphical decrease varies with v. Figure 9 identifies the specific pressurization ΔP that corresponds to the local maximum for $v = 2$. Its value

is $\Delta P = 0.258\mu$. Starting with an unswollen and unpressurized sphere ($v = 1, \Delta P = 0$) consider first an increase in pressure from $\Delta P = 0$ to $\Delta P = 0.258\mu$ while the sphere remains unswollen. The inflation response corresponds to climbing the $v = 1$ curve to $\Delta P = 0.258\mu$ with a relatively small increase in s_i from $s_i = 1$ to $s_i = 1.14$.

Now holding this pressurization fixed let v increase. Then one may proceed in sequence through all of the curves from the original $v = 1$ curve to the curve for $v = 2$. During this sequence there is a corresponding continuous increase in s_i. However, increasing v beyond $v = 2$ cannot proceed with a continuous increase in s_i because the local maximum signals the onset of an interval in s_i corresponding to $v < 2$. This interval proceeds from $s_i = 2.37$ to $s_i = 4.32$. While this interval precludes a continuous increase in s_i as v increases through $v = 2$ it does permit a discontinuous increase from $s_i = 2.37$ to $s_i = 4.32$ at $v = 2$. After such a jump in s_i it is then again possible for s_i to increase continuously because the inflation graphs again become ordered so as permit s_i to increase with v. Figure 10 shows directly the corresponding radial increase with swelling (s_i as a function of v).

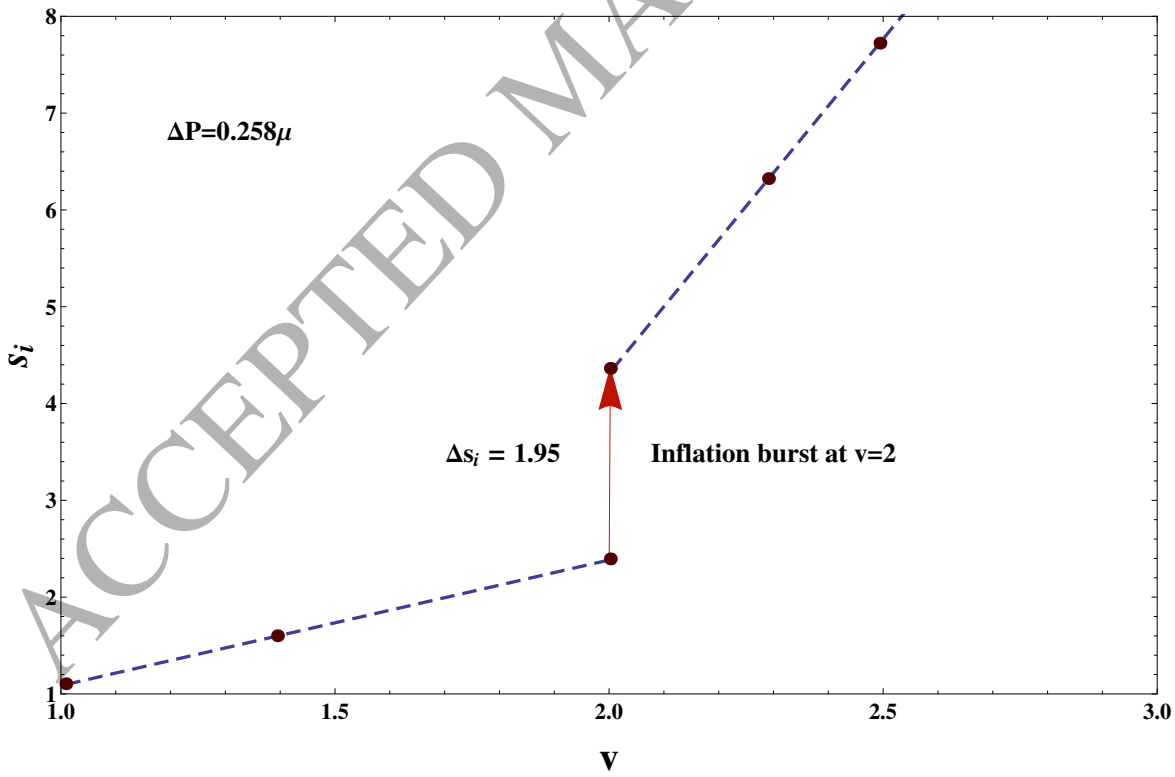

Figure 10: Inflation burst showing $s_i = r_i/R_i$ vs. v at $\Delta P = 0.258\mu$ caused by an increase in the swelling parameter v. Locations denoted by • provide correlation with the inflation graphs depicted in Figure 9.

The jump in s_i corresponds to a "burst of inflation" of limited extent (it concludes at $s_i = 4.32$). Such a burst, which can also be described as a snap-through, is due to the presence of a local maximum in the sequence of inflation graphs. This gives multi-valued choices for s_i when an inflation graph exhibits two increasing branches separated by a decreasing branch.

Under such circumstances some kind of burst is inherent in the mechanical description. However, the description is potentially ambiguous as regards the value of v at which the jump occurs. For example, we have just described a jump from $s_i = 2.37$ to $s_i = 4.32$ when both $\Delta P = 0.258\mu$ and $v = 2$. However, for $\Delta P = 0.258\mu$ the inflation graphs become multi-valued in s_i for values of $v < 2$ and so the question arises, "why not jump before $v = 2$?". In other words, while $v = 2$ is the maximum value of v that permits one to avoid a discontinuity, there is always the possibility of executing an earlier jump.

Such issues have been extensively studied in conventional hyperelasticity Müller & Strehlow (2004) (i.e., no swelling). Then for a single type (c) inflation graph an increase in ΔP eventually provokes a jump to the second increasing branch for the simple reason that the first increasing branch has a maximum permissible ΔP value. This jump could occur at the local maximum or it could occur before the local maximum. Viewing such jumps as a type of phase transition it can be shown that an energy minimal quasi-static process of ΔP increase predicts that the transition occurs prior to attaining the maximum. Specifically it occurs at the value of ΔP associated with the "Maxwell line" construction Ericksen (1975). On the other hand, a transition that occurs at the local maximum upon loading (and at the local minimum upon unloading) is consistent with a notion that the prevailing phase can, under carefully controlled conditions, be preserved even though distantly related states of deformation may now lower the system free energy. In other words, if the system is not subject to large disturbances then jumps will occur at extrema of the inflation graph because it is only then that the inevitable small disturbances provoke a jump to a more energetically favorable configuration.

Such considerations continue to apply to the notion of swelling induced burst that we have been describing. In particular, the sequence of inflation graphs depicted in Figure 6 leads to a situation where, at fixed ΔP, a continuous increase in v will give some kind of abrupt change in inflation. Whether this occurs at the local maximum of an inflation graph or whether it occurs prior to such a local maximum is then to be answered on the basis of a more refined

treatment. This includes energetic stability analysis such as that described in Ericksen (1975) as well as the consideration of less symmetric deformations (such as those with new modes of localized deformation Kyriakides & Chang (1990)). More generally, one can employ a broader thermodynamic framework that allows for supplemental physical considerations (e.g., an additional kinetic relation), as well as additional theoretical considerations from the outset (e.g., inertial dynamics, finer scale physics, a statistical physics treatment of fluctuations). Finally, it is worth remarking that the notion of pressure control is itself likely to be an idealization, and that other forms of control, such as one based on controlling a set mass of sealed in gas Alexander (1971), can lead to different predictions on how transitions occur between different points on an inflation graph.

The inflation burst illustrated in Figure 9 was based on the inflation graphs for the case that was presented in Figure 6. In that case all of the inflation graphs for $v \geq 1$ involved type (c) behavior. Thus one could possibly argue that the swelling induced burst could have been anticipated on the basis of the original unswollen $v = 1$ inflation graph. However, in general it would be premature to draw conclusions on either the presence or absence of swelling induced burst just on the basis of the $v = 1$ inflation graph.

For example, the unswollen $v = 1$ inflation graph in Figure 7 exhibits type (a) behavior. Thus if $v = 1$ then a continuous increase in pressure will result in a continuous expansion and so by itself provides no indication of a burst possibility. However swelling induced inflation burst can still occur. This is shown in Figure 11 for the example of Figure 7. Starting on the $v = 1$ inflation graph with $\Delta P = 1.16\mu$ we consider a subsequent increase in v. The value $\Delta P = 1.16\mu$ is chosen for this discussion because it gives the local maximum on the $v = 2$ inflation graph (other values could similarly be considered). Holding ΔP at this fixed value, an inflation burst is triggered at $v = 2$ in a manner similar to that previously depicted in the example of Figures 9 and 10. In that previous example the inflation graph behavior was type (c) for all values of ΔP prior to the burst. In the present example, the swelling induced burst involves inflation graphs that transition from "benign" type (a) graphs to "burstible" type (c) graphs as the swelling proceeds.

A converse phenomena is also possible if the $v = 1$ unswollen graph is type (c) and which then transitions to type (a) as the swelling proceeds. This was the case for $(\xi, \alpha, p, q) = (0.7, 0.85, 0, 2/3)$ that was discussed in Section 5.3 right after equation (61). In such a case it is found that certain loading sequences which alternate pressurization with strategically placed episodes of swelling and deswelling enable *burst avoidance*. This contrasts with the

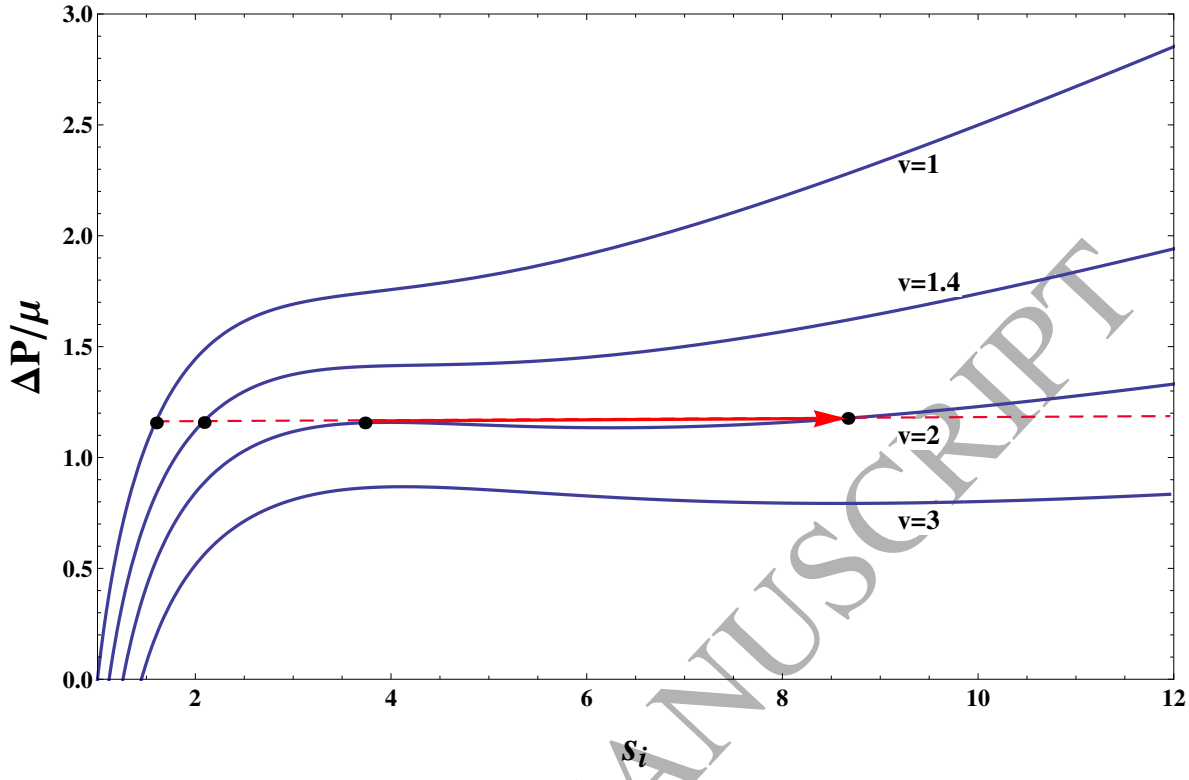

Figure 11: Inflation burst caused by increasing v at fixed $\Delta P = 1.16\mu$ for the inflation graphs from Fig. 7. Initially, the radius increases continuously, first with $v = 1$ as ΔP increases from zero to 1.16μ and then at this fixed ΔP as v increases to $v = 2$ (dashed red segment). At $v = 2$ there is a jump from the first increasing branch to the second increasing branch after which a continuous increase is again the case.

inevitability of burst if all of the pressurization takes place at fixed v.

7. Concluding Remarks

The combined effect of external loading and internal swelling can give rise to complicated states of deformation. Even in the simple setting of a spherical shell subject to combinations of simple pressure with uniform through-thickness (homogeneous) swelling, instabilities can arise that might not otherwise be present if either pressurization or swelling was acting by itself. Here we have investigated the role that swelling can have on eliciting qualitative changes in the pressure-expansion inflation response. Generalizing methods of analysis pioneered by Carroll in the context of incompressible hyperelasticity we have examined a rather straight forward constitutive model, one which is motivated by the well known Mooney-Rivlin model in the incompressible theory, so as to incorporate swelling dependent stiffness parameters. We have shown how certain dependencies preserve the overall qualitative nature of the in-

flation process independent of the amount of swelling, whereas other dependencies do not. In the latter case we have provided general rules, illustrated with examples, showing how certain constitutive forms cause a monotonic (benign) inflation response in the absence of swelling to become nonmonotonic (burst-inducing) as the swelling proceeds. Alternative constitutive forms have the opposite effect, burst-inducing inflation response in the absence of swelling can be mitigated into benign inflation response as the swelling proceeds.

The present study has been limited to the consideration of spherical symmetry. Bifurcations away from spherical symmetry have been extensively studied in the hyperelastic theory, again in the absence of swelling. In particular, the identification of locations on the inflation graph where such bifurcations may initiate can be found by treating an incremental aspherical deformation superimposed on the original spherically symmetric finite deformation. The resulting incremental equations are developed in Haughton & Ogden (1978) for both shells of finite thickness and in the thin membrane limit. The membrane specialization especially permits powerful analysis techniques that allow one to not only identify the initiation of aspherical modes, but to also gauge the relative stability of one branch with respect to another (see Chen & Healey (1991) for a detailed analysis of the spherical solution vs. the branch of "pear shaped" solutions). More recently, highly refined shooting methods have been employed to follow the various solution branches so as to assess how they connect to each other, and how their relative stability can be determined under a variety of controlling situations Fu & Xie (2014). The study here has focused on shells of finite thickness, and so does not make use of the special membrane theory limit, and the elegant procedures that this permits. Finally, returning to the case of finite thickness shells, recent work in the incompressible hyperelastic theory Bustamante & Dorfmann (2013) has uncovered the rich possibilities for different orderings of the various aspherical bifurcation modes that can occur under various modifications of the hyperelastic energy density function – both quantitatively (one term Ogden vs. two term Ogden) and qualitatively (standard energy forms vs. those with limited chain extensibility). Returning to the issue of swelling, the development of surface roughness due to swelling has been observed in solid hydrogel spheres. This may then give way to an aspherical and facetted surface morphology as the swelling proceeds Bertrand et al. (2016). These are typically confined to distinct ranges of overall swelling and may be connected to nonuniform states of internal hydration ($v = v(R)$ in the notation of the present paper), especially if the identified swelling ranges differ on the basis of whether the overall fluid content is increasing or decreasing.

The overall considerations of the present study, as well as possible future studies that bring to bear the techniques in the above referenced works, give rise to the prospect that swelling, when viewed as a control variable, could be manipulated so as to tune the inflation response of spherical shells and membranes. This includes the possibility of both triggering and avoiding instances of inflation burst. On this basis, one may even speculate to what extent such processes of regulation might be present in biological systems. For example, colonies of soft celled creatures are capable of rapidly undergoing complex shape changes. This includes the green alga volvox in the shape of a spherical shell. At a crucial point in their embryonic development, volvox essentially turn themselves inside-out in a process that is conjectured to be triggered by cell shape change at a specific latitude on the shell Höhn et al. (2015); Haas & Goldstein (2015). An intriguing issue in this context is the extent to which the global conditions of the type examined here might possibly abet the resulting snap-through process.

Appendix A. Appendix: Effect of the constitutive exponents p and q on the transitional swelling value $v_{a/c}$

The inflation graph of ΔP vs. s_i for the Mooney-Rivlin swelling model that combines (6) with (56) displays either type (a) or type (c) behavior depending on the thickness ratio $\xi = R_i/R_o$ and the swelling value v. If for fixed ξ it is possible that v alone can cause such a transition, then this transition happens when $v = v_{a/c}$. The transition value $v_{a/c}$ is sensitive to the constitutive parameters α, p and q in (56), however it is not sensitive to μ.

In (61) it is stated that the connection between the function $v_{a/c}$ and the function $v_{A\leftrightarrow C}$ is

$$v_{a/c}(\xi, p-q, \alpha)\Big|_{\xi=1} = v_{A\leftrightarrow C}(p-q, \alpha). \tag{61}$$

This can be understood as follows: type (c) behavior is associated with a graph for G that is not monotonic. Any transition from a monotonic graph to a nonmonotonic graph for G must take place at a value of v for which the graph develops an inflection point with zero slope. The condition for this determines $v_{A\leftrightarrow C}$. On the other hand for a finite thickness shell the condition that determines $v_{a/c}$ is the simultaneous solution of (48) and (49). The conditions (48) and (49) depend on the thickness ratio ξ because this dictates the amount that the graph of G shifts to the left in order to generate the H graph. This shift becomes vanishingly small in the thin shell limit $\xi \to 1$. In order for the match condition (48) to hold under a vanishingly small shift it is required that any such location is one at which the graph of G has zero slope. Similarly, for the matching slope condition (49) to hold under a vanishingly small shift requires a zero curvature location. A location with both zero slope and zero curvature is the defining condition for $v_{A\leftrightarrow C}$. Consequently, $v_{A\leftrightarrow C}$ is the same as $v_{a/c}$ in the thin shell limit $\xi = 1$.

For a finite thickness shell ($\xi < 1$) the values of $v_{A\leftrightarrow C}$ and $v_{a/c}$ will no longer be the same. Here it is useful to recall the diagram in Figure 4 which, for $v = 1$, served to determine the specific thickness ratio ξ associated with the (a) to (c) behavior transition for values of α that were in the special range permitting both behaviors. When swelling is present any such transition is sensitive to both ξ and v. It is then useful to construct curves of $v_{a/c}$ as a function of the structural parameter ξ for fixed material parameters α, p, q. Given a particular shell geometry constructed of a specific material, one can then locate the appropriate point on such a $v_{a/c}$ curve for the purpose of determining the transitional swelling value. The form of these curves are qualitatively different depending on whether $p > q$ or $p < q$. We now

describe in more detail these two separate cases.

Appendix A.1. Dependence of $v_{a/c}$ on ξ for $p > q$

If $p > q$ then the Mooney-Rivlin swelling model (6) with (56) gives $v_{a/c} > v_{A\leftrightarrow C}$. The sphere exhibits type (a) behavior for $v < v_{a/c}$ and type (c) behavior for $v > v_{a/c}$. For fixed constitutive parameters α, p, q the difference $|v_{a/c} - v_{A\leftrightarrow C}|$ decreases for relatively thinner shells (i.e., as $\xi = R_i/R_o$ increases). In particular, $v_{a/c} \to v_{A\leftrightarrow C}$ as $\xi \to 1$.

These features are apparent in Figure A.12 which plots the dependence of $v_{a/c}$ upon ξ for exponent choices $p = 2/3$ and $q = 0$. Because $v_{a/c}$ depends on p and q only through their difference, the Fig. A.12 plots apply more generally to any p and q values obeying $p - q = 2/3$. The different curves correspond to different values of α. Each curve is monotonically decreasing from infinity (as $\xi \to 0$) to the value of $v_{A\leftrightarrow C}$ at $\xi = 1$. Curves for values of $\alpha > 0.823$ are everywhere above the line $v_{a/c} = 1$. This is because $v_{A\leftrightarrow C} > 1$ when $\alpha > 0.823$. In contrast, because $\alpha < 0.823$ makes $v_{A\leftrightarrow C} < 1$ it follows that the curves for $\alpha < 0.823$ cut the line $v = 1$. Because we limit attention to $v \geq 1$ the portions that continue into $v < 1$ are shown as dashed.

The α value of 0.823 *is the value of α_{cr} that was first introduced in (54) in the context of the standard neo-Hookean model.* By virtue of (61) it also serves to make $v_{A\leftrightarrow C}(p-q, \alpha_{cr}) = 1$ because of the direct way in which the standard incompressible model ((5) with (52)) was generalized to the swelling model ((6) with (56)).

The curves shown in Figure A.12 correspond to $p - q = 2/3$. Curves with similar qualitative behavior are obtained provided that $p > q$. In particular, the α value of 0.823 is always associated with $v_{A\leftrightarrow C} = 1$. Spherical shells with $p > q$ and $\alpha > 0.823$ have $v_{a/c} > 1$. They exhibit type (a) behavior for $1 \leq v < v_{a/c}$ and exhibit type (c) behavior for for $v > v_{a/c}$.

Appendix A.2. Dependence of $v_{a/c}$ on ξ for $p < q$

One may similarly construct curves of $v_{a/c}$ vs. ξ for the case in which $p < q$. Now the curves are increasing with ξ instead of decreasing. Each curve continues to approach the value $v_{A\leftrightarrow C}$ as $\xi \to 1$, however now they increase from the value zero at $\xi = 0$. The other major difference is in the significance of these curves. Namely, the spherical shells now have a type (a) behavior in the region *above* the curves ($v > v_{a/c}$) and have a type (c) behavior in the region *below* the curves ($v < v_{a/c}$).

Such curves are displayed in Figure A.13 which plots the dependence of $v_{a/c}$ upon ξ for exponent choices $p = 0$ and $q = 2/3$. More generally this figure also applies to any

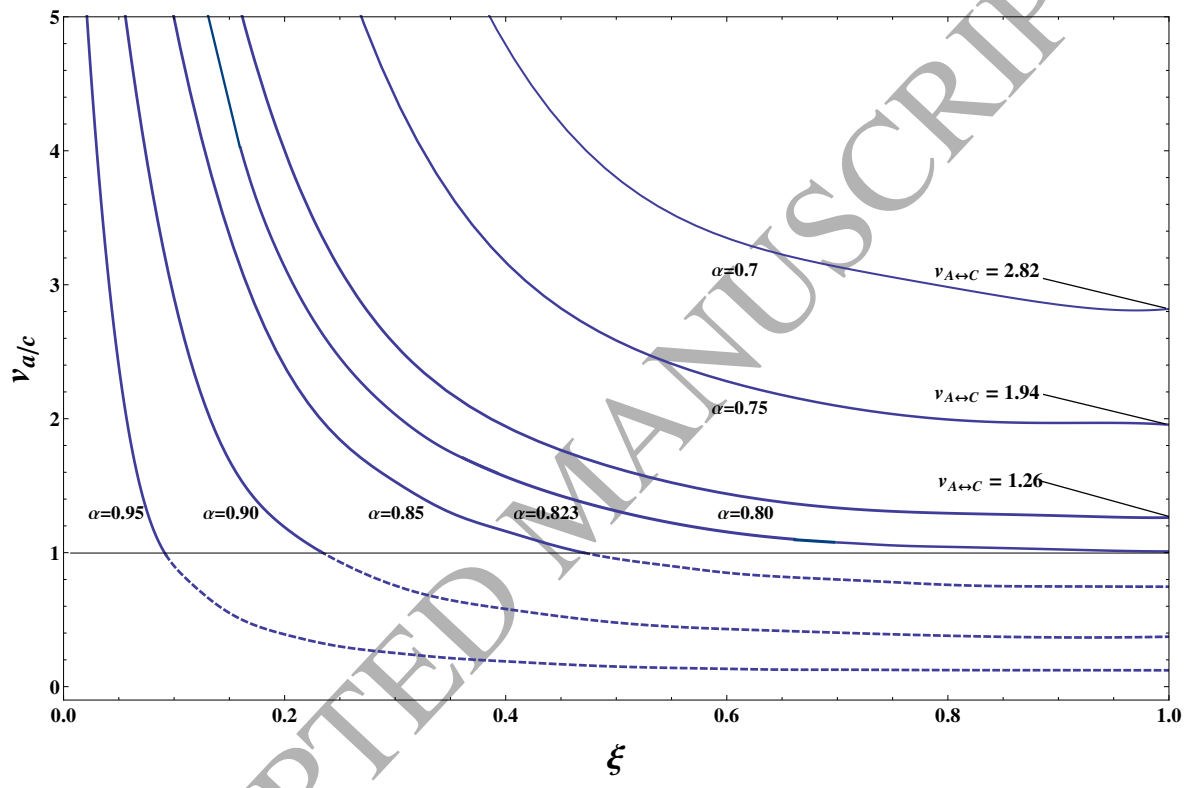

Figure A.12: Transitional swelling value $v_{a/c}$ versus $\xi = R_i/R_o$ for the Mooney-Rivlin-type model (6) with parameters μ, α, p and q in (56). The transitional swelling value $v_{a/c}$ is independent of μ and is dependent on p and q only via the difference $p - q$. These plots are for $p - q = 2/3$. For a given α-curve the inflation graph exhibits type (c) behavior if (ξ, v) is in the region above the curve and type (a) behavior if (ξ, v) is in the region below the curve.

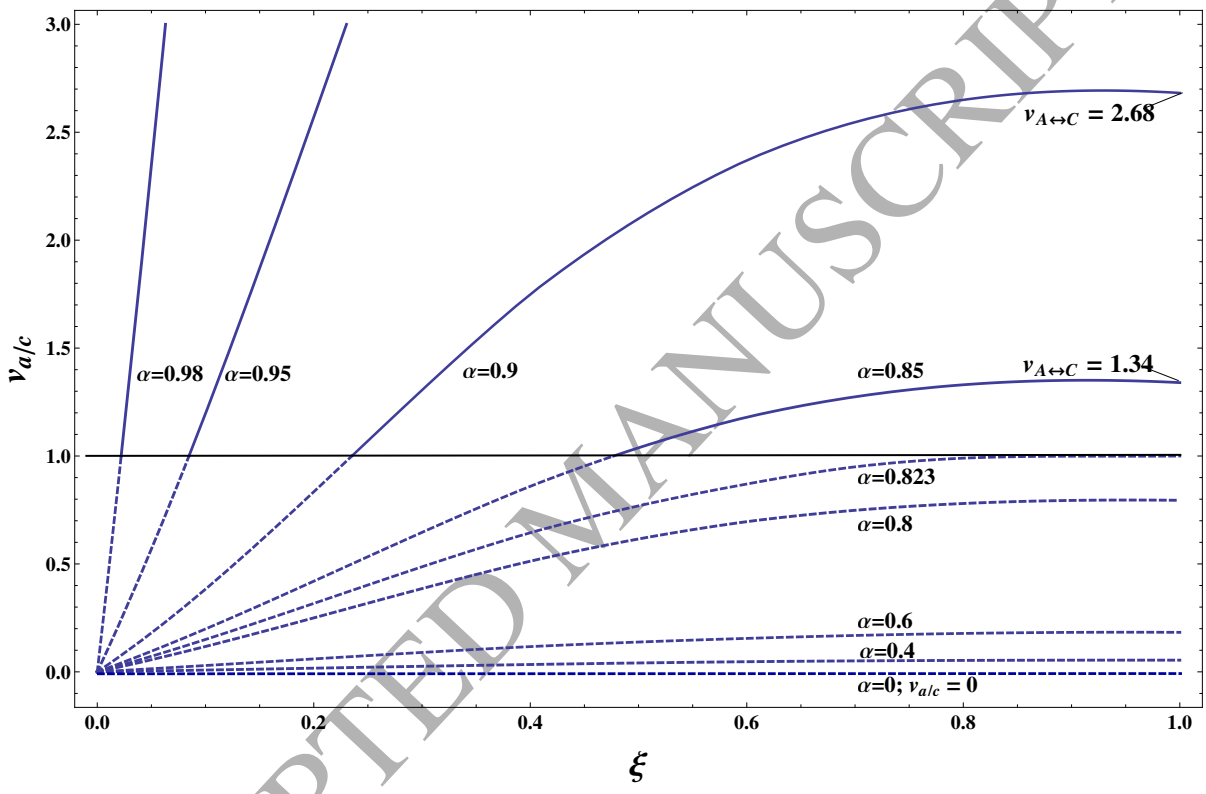

Figure A.13: Transitional values for swelling $v_{a/c}$ versus $\xi = R_i/R_o$ for Mooney-Rivlin-type model (6) with parameters μ, α, p and q in (56). The transitional swelling value $v_{a/c}$ is dependent on α as shown but is independent of μ. The curves are dependent on p and q only via the difference $p - q$. This figure is for $p - q = -2/3$. For a given α-curve the inflation graph exhibits type (c) behavior when (ξ, v) is in the region that is below the curve and type (a) behavior in the region that is above the curve.

p and q values obeying $p - q = -2/3$. Qualitatively similar curves hold for any p and q obeying $p < q$. The value $\alpha = 0.823$ continues to retain its special significance because of its continued association with the condition $v_{A\leftrightarrow C} = 1$. It is now the case that curves for $\alpha < 0.823$ are always confined to the region $v_{a/c} < 1$. Because the condition $v < 1$ is not being considered, the $\alpha < 0.823$ curves are shown as dashed over their entire length. Thus if $\alpha < 0.823$ (and $p < q$) then any spherical shell has type (a) behavior for $v \geq 1$.

Conversely curves for $\alpha > 0.823$ cut the line $v = 1$. The portions of these curves that are below the value $v = 1$ are again shown as dashed. If $\alpha > 0.823$ and the shell is sufficiently thick then it has a type (a) inflation graph for all $v \geq 1$; this is because $v_{a/c} < 1$. However if the shell is sufficiently thin then $v_{a/c} > 1$; this means that it has a type (c) inflation graph for $1 \leq v < v_{a/c}$ and a type (a) inflation graph for $v > v_{a/c}$. Consequently in such a case a quasi-static increase in v from the unswollen state $v = 1$ will generate a transition from type (c) to type (a) behavior as v passes through the special value $v_{a/c}$.

Acknowledgment: This work is made possible by NPRP grant no. 4-1333-1-214 from the Qatar National Research Fund (a member of Qatar Foundation). The statements made herein are solely the responsibility of the authors.

References

Alexander, H. (1971). Tensile instability of initially spherical balloons. *International Journal of Engineering Science*, *9*, 151–160.

Ben Amar, M., & Goriely, A. (2005). Growth and instability in elastic tissues. *Journal of the Mechanics and Physics of Solids*, *53*, 2284–2319.

Bertrand, T., Peixinho, J., Mukhopadhyay, S., & MacMinn, C. W. (2016). Dynamics of swelling and drying in a spherical gel. *Physical Review Applied*, *6*, 064010.

Bustamante, R., & Dorfmann, A. (2013). Axisymmetric bifurcations of thick spherical shells under inflation and compression. *International Journal of Solids and Structures*, *50*, 403–413.

Carroll, M. M. (1987). Pressure maximum behavior in inflation of incompressible elastic hollow spheres and cylinders. *Quarterly of applied mathematics*, *45*, 141–154.

Chen, Y.-C., & Healey, T. J. (1991). Bifurcation to pear-shaped equilibria of pressurized spherical membranes. *International Journal of Non-Linear Mechanics*, *26*, 279–291.

Demirkoparan, H., & Pence, T. J. (2008). Torsional swelling of a hyperelastic tube with helically wound reinforcement. *Journal of Elasticity*, *92*, 61–90.

Drozdov, A. D. (2013). Finite elasticity of nanocomposite hydrogels. *Composite Interfaces*, *20*, 673–692.

Ericksen, J. L. (1975). Equilibrium of bars. *Journal of Elasticity*, *5*, 191–201.

Evans, E., Heinrich, V., Ludwig, F., & Rawicz, W. (2003). Dynamic tension spectroscopy and strength of biomembranes. *Biophysical Journal*, *85*, 2342–2350.

Fu, Y. B., & Xie, Y. X. (2014). Stability of pear-shaped configurations bifurcated from a pressurized spherical balloon. *Journal of the Mechanics and Physics of Solids*, *68*, 33–44.

Gibbons, M. M., & Klug, W. S. (2008). Influence of nonuniform geometry on nanoindentation of viral capsids. *Biophysical Journal*, *95*, 3640–3649.

Goriely, A., Moulton, D. E., & Vandiver, R. (2010). Elastic cavitation, tube hollowing, and differential growth in plants and biological tissues. *EPL (Europhysics Letters)*, *91*, 18001.

Graf, J., Rupnik, M., Zupancic, G., & Zorec, R. (1995). Osmotic swelling of hepatocytes increases membrane conductance but not membrane capacitance. *Biophysical Journal*, *68*, 1359.

Green, A. E., & Shield, R. T. (1950). Finite elastic deformation of incompressible isotropic bodies. In *Proceedings of the Royal Society of London A: Mathematical, Physical and Engineering Sciences* (pp. 407–419). The Royal Society volume 202.

Haas, P. A., & Goldstein, R. E. (2015). Elasticity and glocality: initiation of embryonic inversion in volvox. *Journal of The Royal Society Interface*, *12*, 20150671.

Haughton, D. M., & Ogden, R. W. (1978). On the incremental equations in non-linear elasticity–II. Bifurcation of pressurized spherical shells. *Journal of the Mechanics and Physics of Solids*, *26*, 111–138.

Höhn, S., Honerkamp-Smith, A. R., Haas, P. A., Trong, P. K., & Goldstein, R. E. (2015). Dynamics of a volvox embryo turning itself inside out. *Physical Review Letters*, *114*, 178101.

Kyriakides, S., & Chang, Y.-C. (1990). On the inflation of a long elastic tube in the presence of axial load. *International Journal of Solids and Structures*, *26*, 975–991.

Li, F., Chan, C. U., & Ohl, C. D. (2013). Yield strength of human erythrocyte membranes to impulsive stretching. *Biophysical Journal*, *105*, 872–879.

Müller, I., & Strehlow, P. (2004). *Rubber and rubber balloons: paradigms of thermodynamics* volume 637. Springer Science & Business Media.

Nagel, T., Loerakker, S., & Oomens, C. W. J. (2009). A theoretical model to study the effects of cellular stiffening on the damage evolution in deep tissue injury. *Computer Methods in Biomechanics and Biomedical Engineering*, *12*, 585–597.

Ogden, R. W. (1997). *Non-linear elastic deformations*. Courier Corporation.

Pence, T. J., & Tsai, H. (2005). Swelling-induced microchannel formation in nonlinear elasticity. *IMA Journal of Applied Mathematics*, *70*, 173–189.

Pence, T. J., & Tsai, H. (2006). Swelling-induced cavitation of elastic spheres. *Mathematics and Mechanics of Solids*, *11*, 527–551.

Sadik, S., Angoshtari, A., Goriely, A., & Yavari, A. (2016). A geometric theory of nonlinear morphoelastic shells. *Journal of Nonlinear Science*, *26*, 929–978.

Van der Sman, R. G. M. (2015). Hyperelastic models for hydration of cellular tissue. *Soft Matter*, *11*, 7579–7591.

Stuart, M. A. C., Huck, W. T. S., Genzer, J., Müller, M., Ober, C., Stamm, M., Sukhorukov, G. B., Szleifer, I., Tsukruk, V. V., Urban, M. et al. (2010). Emerging applications of stimuli-responsive polymer materials. *Nature Materials*, *9*, 101–113.

Treloar, L. R. G. (1975). *The physics of rubber elasticity*. Oxford University Press, USA.

Tsai, H., Pence, T. J., & Kirkinis, E. (2004). Swelling induced finite strain flexure in a rectangular block of an isotropic elastic material. *Journal of Elasticity*, *75*, 69–89.

Vinod Kumar, K., & Demeke, F. (2011). Analysis of mechanical behavior of red blood cell membrane with malaria infection. *World Journal of Mechanics*, *2011*.